PAPER

The Talbot effect in a two-dimensional system with Rashba spin–orbit coupling

IOP Publishing Physica Scripta
Phys. Scr. 95 (2020) 025005 (15pp) https://doi.org/10.1088/1402-4896/ab4208

The Talbot effect in a two-dimensional system with Rashba spin–orbit coupling

Jamie D Walls and Zhaoyuan Gong

Department of Chemistry, University of Miami, Coral Gables, Florida 33124, United States of America

E-mail: jwalls@miami.edu

Received 9 May 2019, revised 21 August 2019
Accepted for publication 6 September 2019
Published 3 January 2020

Abstract

In this work, a theory for the scattering of two-dimensional plane-waves from a periodic, quasi-one-dimensional array of nonmagnetic, localized scatterers in the presence of Rashba spin–orbit coupling is presented. Formulas for the spin-subband resolved transmission and reflection coefficients along with the transmitted and reflected wave functions are derived. In the presence of spin–orbit coupling, the Talbot effect, where periodic modulations in the transmitted probability density arise along a direction orthogonal to the periodic direction of the scattering potential, is shown to occur. However, it is demonstrated that Rashba spin–orbit coupling increases the complexity of the observed interference patterns where different types of Talbot lengths due to both *interspin* and *intraspin* subband scattering are predicted. Numerical calculations are provided to support the theoretical calculations presented in this work.

Keywords: spin–orbit coupling, Talbot effect, scattering theory

(Some figures may appear in colour only in the online journal)

1. Introduction

It has long been appreciated [1] that making connections to classical optical phenomena can help in understanding coherent transport and related interference phenomena in delocalized electronic systems, such as found for a two-dimensional electron gas (2DEG) in semiconductor heterostructures. For example, optical analogs for coherent scattering and/or transport in electronic systems provide a simple framework for understanding the observed interference patterns in scanning tunneling microscopic (STM) images of quantum corrals on metal surfaces [2, 3] and in conductance imaging measurements in 2DEGs [4, 5]. One important optical phenomenon where fruitful analogies to electron dynamics could exist is the Talbot effect [6–8]. In the Talbot effect, a monochromatic wave with wavelength λ that is normally incident to a periodic diffraction grating with lattice constant $d \gg \lambda$ will result in a transmitted wave that is periodically refocused away from the diffraction grating at integer multiples of the Talbot length, $z_T = \frac{2d^2}{\lambda}$. The interference patterns observed in the Talbot effect are a result of coherent transport through the diffraction grating that is intimately connected to the theory of quantum revivals [9]. While normally viewed as an optical phenomenon, the Talbot effect can manifest itself whenever there is coherent scattering of waves from a periodic potential, such as in the scattering of electrons [10], atoms [11], and molecules [12] from a periodic diffraction grating. In two-dimensional systems, the plasmon Talbot effect [13, 14] has been observed along with proposals for an electron spin Talbot effect in 2DEGs [15] and a Talbot effect for massless Dirac fermions found in single layer graphene [16]. When $d \gg \lambda$, all of the aforementioned theoretical and experimental studies of the Talbot effect predict that the refocusing of the transmitted waves from a periodic diffraction grating can be described by a single Talbot length, z_T.

While previous work [13–16] has explored the Talbot effect in a variety of two-dimensional systems as mentioned above, the effects of spin–orbit coupling on the Talbot effect have remain unexplored. In particular, Rashba spin–orbit coupling [17], where both spin and linear momentum are coupled due to the asymmetry of the confining potential along the third dimension, has been predicted to modify the observed interference patterns for STM images of quantum corrals on the Au(III) surface [18] and for conductance imaging measurements in 2DEGs [19], all of which suggests that Rashba spin–orbit coupling may also alter the observed Talbot effect in such systems. Theoretical studies on the effects of periodic, two-dimensional electrostatic potentials on band

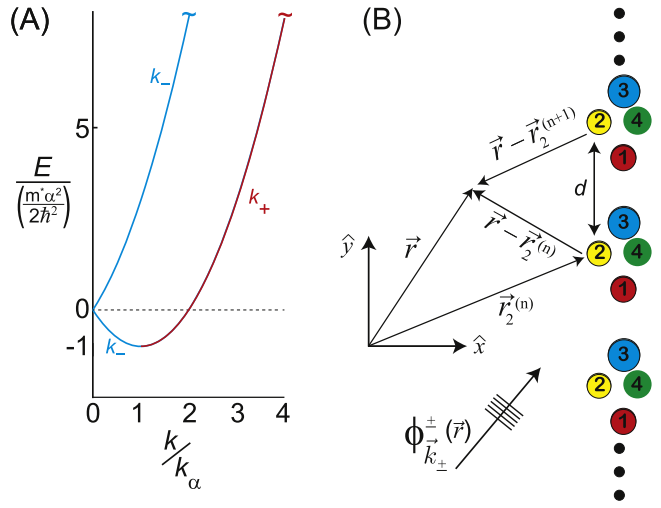

Figure 1. (A) The E versus $k_\pm$ dispersion relationships for the '$\pm$'-spin subbands of a two-dimensional particle with effective mass m^* in the presence of Rashba spin–orbit interaction ($\widehat{H}_0$ in equation (1)). For $E > 0$, spin–orbit coupling results in a constant difference in wave vector magnitudes between the '+'-spin subband (k_+, red dispersion curve) and the '−'-spin subband (k_-, blue dispersion curve) of $k_+ - k_- = 2k_\alpha = \frac{2m^*\alpha^2}{\hbar^2}$. (B) Scattering of an incident wave in the '$\pm$'-spin subband, $\phi^{\pm}_{\vec{k}_\pm}(\vec{r})$, from a periodic, quasi-one-dimensional potential with lattice constant d, $\widehat{V}(\vec{r})$ in equation (4). For the scattering array illustrated in (B), the unit cell consists of four scatterers ($N_s = 4$) with the position of the mth scatterer in the nth unit cell given by $\vec{r}_m^{(n)} = \vec{r}_m + nd\hat{y}$.

structure and spin texture in systems with Rashba spin–orbit coupling have also been extensively studied [20–23] along with the effects of periodically modulating the Rashba coupling strength [24]; however, none of these studies have focused on a periodic, quasi-one-dimensional scattering potential like the one illustrated in figure 1(B) that would be relevant to studying the Talbot effect.

For an energy $E > 0$, there are two different wavelengths or 'colors' due to spin–orbit coupling that are associated with the '$\pm$'-spin subbands, λ_+ and λ_-, respectively. A wave of a given wavelength/color, $\lambda_\pm$, that is incident to a nonmagnetic diffraction grating generates a transmitted wave consisting of up to two colors due to *interspin* subband scattering from the potential, λ_+ and λ_-. As a result, the interference patterns in the transmitted probability density become more complex due to spin–orbit coupling and may contain two different types of Talbot lengths: those due to *intraspin* subband interference in the '$\pm$'-spin subbands and those due to *interspin* subband interference. This type of 'multicolor' Talbot effect, which is the result of spin–orbit coupling, is unique from previous systems where the 'monochromatic' Talbot effect has been investigated. Furthermore, results from this work could be useful to experimentalists studying coherent transport in a wide range of effective two-dimensional systems, e.g., noble metal surfaces, 2DEGs, photonic lattices, etc., where the dynamics can be 'engineered' in such a way that the system evolves under an 'effective' Rashba spin–orbit interaction.

This paper is organized as follows: the basic theory for two-dimensional multiple scattering of an incident wave from a periodic, quasi-one-dimensional array of localized, nonmagnetic scatterers in the presence of Rashba spin–orbit coupling is presented in section 2. Formulas for both the spin-subband resolved transmission and reflection coefficients along with numerical simulations are given in section 2.1, which is followed by a discussion of the transmitted probability density in section 2.2. The theory for the Talbot effect in the presence of Rashba spin–orbit coupling is given in section 3 where it is shown through both numerical and theoretical calculations that different Talbot lengths due to *intraspin* and *interspin* subband interference should be observable. Conclusions are presented in section 4 followed by additional derivations and details of the multiple scattering calculations presented in the appendices.

2. Theory

The Hamiltonian for a particle in two-dimensions (e.g. a 2DEG) in the presence of the Rashba spin–orbit interaction and a two-dimensional electrostatic potential, $\widehat{V}(\vec{r})$, is given by

$$\begin{aligned}\widehat{H} &= \frac{\widehat{p}_X^2}{2m^*} + \frac{\widehat{p}_Y^2}{2m^*} - \frac{\alpha}{\hbar}(\widehat{p}_Y\widehat{\sigma}_X - \widehat{p}_X\widehat{\sigma}_Y) + \widehat{V}(\vec{r}) \\ &= \widehat{H}_0 + \widehat{V}(\vec{r}),\end{aligned} \tag{1}$$

where $\widehat{\sigma}_j$ are the Pauli spin matrices, m^* is the effective mass, and α is the Rashba spin–orbit coupling constant (taken in this work to be a positive quantity). For a free particle [$\widehat{V}(\vec{r}) = 0$], the dispersion relation for $\widehat{H} = \widehat{H}_0$ in equation (1) consists of two, spin–split parabolic bands with wave vector magnitudes, $k_+ \equiv k_1$ and $k_- \equiv k_2$ (the red and blue curves shown in figure 1(A), respectively), which are given by:

$$\begin{aligned}k_\pm &= \overline{k} \pm k_\alpha \quad \text{for } E \geqslant 0 \\ k_\pm &= k_\alpha \pm \overline{k} \quad \text{for } -\frac{\hbar^2 k_\alpha^2}{2m^*} \leqslant E \leqslant 0,\end{aligned} \tag{2}$$

where $\overline{k} = \sqrt{\frac{2m^*E}{\hbar^2} + \left(\frac{m^*\alpha}{\hbar^2}\right)^2}$ and $k_\alpha = \frac{m^*\alpha}{\hbar^2}$. It has been reported [25] that for Au(111) surface states, $m^* = 0.26m_e$, $\alpha = 4.4 \times 10^{-11}$ eVm, and $k_\alpha = 5.774 \times 10^8$ m^{-1} whereas in InSb nanowires [26], $m^* \approx 0.014m_e$, $\alpha \approx 7.5 \times 10^{-11}$ eVm, and $k_\alpha \approx 1.378 \times 10^7$ m^{-1}. For any $E > 0$, there exists a constant difference in the corresponding wave vector magnitudes of the '$\pm$'-spin subbands that is *independent* of E, $k_1 - k_2 = 2k_\alpha$.

The corresponding eigenstates of $\widehat{H}_0$ at energy E can be written as plane-wave spinors in the '$\pm$'-spin subbands, $\phi^{\pm}_{\vec{k}_\pm}(\vec{r})$, where the $\pm$ superscript of $\phi^{\pm}$ indicates the corresponding spin subband of the plane-wave state with corresponding wave vectors

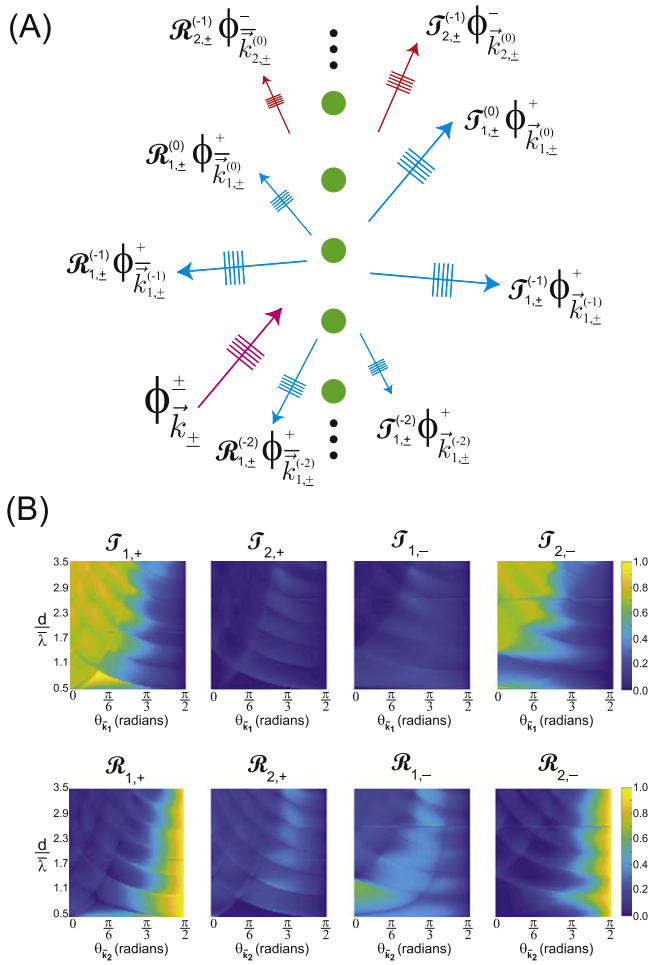

Figure 2. (A) Scattering of an incident plane-wave state, $\phi^{\pm}_{\vec{k}_{\pm}}(\vec{r})$, from a quasi-one-dimensional potential. As depicted in (A), $N_s = 1$, and the open channels were given by $\mathcal{N}_{2,\pm} = \{-1\}$ and $\mathcal{N}_{1,\pm} = \{0, -1, -2\}$. The spin subband-resolved total transmission and reflection probabilities were given by $\mathcal{T}_{1,\pm} = \sum_{n\in\mathcal{N}_{1,\pm}}|\mathcal{T}^{(n)}_{1,\pm}|^2$, $\mathcal{T}_{2,\pm} = \sum_{q\in\mathcal{N}_{2,\pm}}|\mathcal{T}^{(q)}_{2,\pm}|^2$, $\mathcal{R}_{1,\pm} = \sum_{n\in\mathcal{N}_{1,\pm}}|\mathcal{R}^{(n)}_{1,\pm}|^2$, and $\mathcal{R}_{2,\pm} = \sum_{q\in\mathcal{N}_{2,\pm}}|\mathcal{R}^{(q)}_{2,\pm}|^2$. (B) Total spin subband-resolved transmission [$\mathcal{T}_{1,\pm}$ and $\mathcal{T}_{2,\pm}$] and reflection [$\mathcal{R}_{1,\pm}$ and $\mathcal{R}_{2,\pm}$] probabilities for a plane-wave incident to a periodic, quasi-one-dimensional scattering array ($d = 300$ nm) as a function of θ_0 and $\overline{\lambda}$. The scattering array consisted of a single scatterer with $a_1 = 40$ nm and $V_1 = -0.2$ eV. In all simulations, $m^* = 0.014\, m_e$ and $\alpha = 5 \times 10^{-11}$ eVm with $k_\alpha = 9.186 \times 10^6\ \mathrm{m}^{-1}$.

$\vec{k}_{\pm} = (k_{X,\pm})\hat{x} + (k_{Y,\pm})\hat{y} \equiv k_{\pm}(\cos(\theta_{\vec{k}_{\pm}})\hat{x} + \sin(\theta_{\vec{k}_{\pm}})\hat{y})$, where the E dependence of both $\phi^{\pm}_{\vec{k}_{\pm}}(\vec{r})$ and $k_{\pm}$ is not explicitly shown. For $E > 0$, $\phi^{\pm}_{\vec{k}_{\pm}}(\vec{r})$ is given by:

$$\phi^{\pm}_{\vec{k}_{\pm}}(\vec{r}) = \sqrt{\frac{m^*}{2\hbar\bar{k}}}\sqrt{\frac{k_{\pm}}{|\vec{k}_{\pm}\cdot\hat{n}|}}\,\mathrm{e}^{\mathrm{i}\vec{k}_{\pm}\cdot\vec{r}}\begin{pmatrix}1\\ \mp\mathrm{i}\mathrm{e}^{\mathrm{i}\theta_{\vec{k}_{\pm}}}\end{pmatrix} \tag{3}$$

where $\phi^{\pm}_{\vec{k}_{\pm}}(\vec{r})$ is flux-normalized along the $\hat{n}$-direction. In equation (3), $\phi^{+}_{\vec{k}_{+}}(\vec{r}) \equiv \phi^{+}_{\vec{k}_1}(\vec{r})$ is associated with the '+'-spin subband (red dispersion curve in figure 1(A)) while $\phi^{-}_{\vec{k}_{-}}(\vec{r}) \equiv \phi^{-}_{\vec{k}_2}(\vec{r})$ is associated with the '−'-spin subband (blue dispersion curve in figure 1(A)).

2.1. Multiple scattering formalism for a periodic, quasi-one-dimensional scattering array

Consider a $\widehat{V}(\vec{r})$ for a quasi-one-dimensional scattering array that is periodic along the $\hat{y}$-dimension with lattice constant d and with a unit cell consisting of N_s, localized, nonmagnetic, cylindrically symmetric scatterers:

$$\widehat{V}(\vec{r}) = \sum_{n=-\infty}^{\infty}\sum_{m=1}^{N_s} V_m \Theta_{a_m}(\vec{r} - \vec{r}^{(n)}_m), \tag{4}$$

where $\vec{r}^{(n)}_m = \vec{r}_m + nd\hat{y}$ denotes the position of the mth scatterer in the nth unit cell, and a_m and V_m denote the effective radius and strength of the scattering step potential for scatterer m in a unit cell with:

$$\Theta_{a_m}(\vec{r}) = \begin{cases}0 & \text{if } |\vec{r}| > a_m\\ 1 & \text{if } |\vec{r}| \leqslant a_m\end{cases}. \tag{5}$$

In the following, the position of the mth scatterer in the $n = 0$ unit cell is denoted simply by $\vec{r}_m \equiv \vec{r}^{(0)}_m$.

Consider a plane-wave state in the '±'-spin subband with $E > 0$, $\phi^{\pm}_{\vec{k}_{\pm}}(\vec{r})$ in equation (3), that is flux-normalized along the $+\hat{x}$-direction and is incident from the left of the scattering potential, $\widehat{V}(\vec{r})$ in equation (4), i.e. $\phi^{+}_{\vec{k}_{+}}(\vec{r}) = \sqrt{\frac{m^*}{2\hbar\bar{k}\cos(\theta_0)}}\,\mathrm{e}^{\mathrm{i}\vec{k}_{+}\cdot\vec{r}}\begin{pmatrix}1\\ -\mathrm{i}\mathrm{e}^{\mathrm{i}\theta_0}\end{pmatrix}$ or $\phi^{-}_{\vec{k}_{-}}(\vec{r}) = \sqrt{\frac{m^*}{2\hbar\bar{k}\cos(\theta_0)}}\,\mathrm{e}^{\mathrm{i}\vec{k}_{-}\cdot\vec{r}}\begin{pmatrix}1\\ \mathrm{i}\mathrm{e}^{\mathrm{i}\theta_0}\end{pmatrix}$, for $\vec{k}_{\pm} = k_{Y,\pm}\hat{y} + k_{X,\pm}\hat{x} = k_{\pm}(\cos(\theta_0)\hat{x} + \sin(\theta_0)\hat{y})$ with $-\frac{\pi}{2} < \theta_0 < \frac{\pi}{2}$. The total wave function, $\Psi^{\pm}(\vec{r})$, which satisfies $\widehat{H}\Psi^{\pm}(\vec{r}) = E\Psi^{\pm}(\vec{r})$, will consist of the incident plane-wave plus reflected ($x < 0$) and transmitted ($x > 0$) plane-wave states from each spin subband (as illustrated in figure 2(A)). Since the quasi-one-dimensional potential in equation (4) satisfies the relation $\widehat{V}(\vec{r} + pd\hat{y}) = \widehat{V}(\vec{r})$ for integer p, the total wave function must also satisfy $\Psi^{\pm}(\vec{r} + pd\hat{y}) = \Psi^{\pm}(\vec{r})$ as a consequence of Bloch's theorem [27]. As a result, the transmitted plane-wave states ($x \gg d$) in each spin subband, $\phi^{+}_{\vec{k}^{(n)}_{1,\pm}}$ and $\phi^{-}_{\vec{k}^{(q)}_{2,\pm}}$, and reflected plane-wave states ($x \ll -d$), $\phi^{+}_{\vec{k}^{(n)}_{1,\pm}}$ and $\phi^{-}_{\vec{k}^{(q)}_{2,\pm}}$, can be denoted by integers $n \in \mathcal{N}_{1,\pm}$ and $q \in \mathcal{N}_{2,\pm}$, where:

$$\begin{aligned}\mathcal{N}_{1,\pm} &= \left[\left\{-\frac{(k_1 + k_{\pm}\sin(\theta_0))d}{2\pi}\right\}_{+}, \ldots, \left\{\frac{(k_1 - k_{\pm}\sin(\theta_0))d}{2\pi}\right\}_{-}\right]\\ \mathcal{N}_{2,\pm} &= \left[\left\{-\frac{(k_2 + k_{\pm}\sin(\theta_0))d}{2\pi}\right\}_{+}, \ldots, \left\{\frac{(k_2 - k_{\pm}\sin(\theta_0))d}{2\pi}\right\}_{-}\right]\end{aligned} \tag{6}$$

with $\{z\}_{+}$ corresponding to the smallest integer greater than z, and $\{z\}_{-}$ corresponding to the largest integer less than z. The corresponding purely real wave vectors for the transmitted and reflected plane-wave states are given by:

$$\left.\begin{aligned}\vec{k}^{(n)}_{1,\pm} &= k^{(n)}_{Y,\pm}\hat{y} + k^{(n)}_{1X,\pm}\hat{x} = \left(k_{Y,\pm} + \tfrac{2\pi n}{d}\right)\hat{y} + \sqrt{k_1^2 - (k^{(n)}_{Y,\pm})^2}\,\hat{x}\\ \overline{\vec{k}^{(n)}_{1,\pm}} &= k^{(n)}_{Y,\pm}\hat{y} - k^{(n)}_{1X,\pm}\hat{x} = \left(k_{Y,\pm} + \tfrac{2\pi n}{d}\right)\hat{y} - \sqrt{k_1^2 - (k^{(n)}_{Y,\pm})^2}\,\hat{x}\end{aligned}\right\} \; n \in \mathscr{N}_{1,\pm}$$

$$\left.\begin{aligned}\vec{k}^{(q)}_{2,\pm} &= k^{(q)}_{Y,\pm}\hat{y} + k^{(q)}_{2X,\pm}\hat{x} = \left(k_{Y,\pm} + \tfrac{2\pi q}{d}\right)\hat{y} + \sqrt{k_2^2 - (k^{(q)}_{Y,\pm})^2}\,\hat{x}\\ \overline{\vec{k}^{(q)}_{2,\pm}} &= k^{(q)}_{Y,\pm}\hat{y} - k^{(q)}_{2X,\pm}\hat{x} = \left(k_{Y,\pm} + \tfrac{2\pi q}{d}\right)\hat{y} - \sqrt{k_2^2 - (k^{(q)}_{Y,\pm})^2}\,\hat{x}\end{aligned}\right\} \; q \in \mathscr{N}_{2,\pm}. \tag{7}$$

The total wave function $\Psi^{\pm}(\vec{r})$ can be determined self-consistently using multiple scattering theory (details are given in appendix A). Without going into the details of the multiple scattering calculations, however, qualitative information about $\Psi^{\pm}(\vec{r})$ can be obtained by simply determining the nature and existence of the 'open channels' that an incident wave can scatter into. For any incident wave in the '−'-spin subband, both $\mathscr{N}_{2,-} \neq \{\varnothing\}$ and $\mathscr{N}_{1,-} \neq \{\varnothing\}$ since $k_1 > k_2$ for $\alpha > 0$ meaning that there can always be *interspin* subband scattering for an incident wave in the '−'-spin subband. While $\mathscr{N}_{1,+} \neq \{\varnothing\}$ for any incident wave in the '+'-spin subband, it is possible to have $\mathscr{N}_{2,+} = \{\varnothing\}$ for incident waves with $\frac{d}{\lambda_1} \leq \frac{1}{2}$ and $\frac{d}{\lambda_2} < \frac{d}{\lambda_1}|\sin(\theta_0)|$. For $\frac{d}{\lambda_1} > \frac{1}{2}$, $\mathscr{N}_{2,+} = \{\varnothing\}$ when:

$$\frac{d}{\overline{\lambda}} < \begin{cases} \frac{d}{\lambda_\alpha}\frac{1+|\sin(\theta_0)|}{1-|\sin(\theta_0)|} & \text{for } 0 \leqslant |\theta_0| \leqslant \Theta_{\text{inter}} \\ \frac{d}{\lambda_\alpha}\frac{1-|\sin(\theta_0)|+\frac{d}{\lambda_\alpha}}{1+|\sin(\theta_0)|} & \text{for } |\theta_0| \geqslant \Theta_{\text{inter}} \end{cases} \tag{8}$$

where $\overline{\lambda} = \frac{2\pi}{\overline{k}}$, $\lambda_\alpha = \frac{2\pi}{k_\alpha}$, and:

$$\sin(\Theta_{\text{inter}}) = \frac{1}{\frac{4d}{\lambda_\alpha} + 1} \tag{9}$$

in which case *interspin* subband scattering cannot occur.

For $x \gg d$, the total transmitted wave function, $\Psi^{\pm}_{\mathscr{T}}(\vec{r})$, can be written as a sum over all open channels:

$$\Psi^{\pm}_{\mathscr{T}}(\vec{r}) = \sum_{n\in\mathscr{N}_{1,\pm}} \mathscr{T}^{(n)}_{1,\pm}\phi^{+}_{\vec{k}^{(n)}_{1,\pm}}(\vec{r}) + \sum_{p\in\mathscr{N}_{2,\pm}} \mathscr{T}^{(p)}_{2,\pm}\phi^{-}_{\vec{k}^{(p)}_{2,\pm}}(\vec{r}) \tag{10}$$

with the corresponding transmission coefficients given by:

$$\begin{aligned}\mathscr{T}^{(n)}_{1,\pm} &= \delta_{+,\pm}\delta_{n0} + \sum_{m=1}^{N_s}\sum_{l=-l_{\max}}^{l_{\max}} \frac{t_{1;l,a_m}\mathrm{e}^{-\mathrm{i}\vec{k}^{(n)}_{1,\pm}\cdot\vec{r}_m}}{d} \\ &\quad\times\sqrt{\frac{2\hbar\overline{k}}{m^* k_1 k^{(n)}_{1X,\pm}}}\left[\begin{pmatrix}\mathrm{e}^{-\mathrm{i}l\theta_{\vec{k}^{(n)}_{1,\pm}}} \\ \mathrm{i}\mathrm{e}^{\mathrm{i}(l-1)\theta_{\vec{k}^{(n)}_{1,\pm}}}\end{pmatrix}\right]^{\mathrm{T}}\widehat{T}_l\Psi^{\pm}(\vec{r}_m) \\ \mathscr{T}^{(n)}_{2,\pm} &= \delta_{-,\pm}\delta_{n0} + \sum_{m=1}^{N_s}\sum_{l=-l_{\max}}^{l_{\max}} \frac{t_{2;l,a_m}\mathrm{e}^{-\mathrm{i}\vec{k}^{(n)}_{2,\pm}\cdot\vec{r}_m}}{d} \\ &\quad\times\sqrt{\frac{2\hbar\overline{k}}{m^* k_2 k^{(n)}_{2X,\pm}}}\left[\begin{pmatrix}\mathrm{e}^{-\mathrm{i}l\theta_{\vec{k}^{(n)}_{2,\pm}}} \\ -\mathrm{i}\mathrm{e}^{\mathrm{i}(l-1)\theta_{\vec{k}^{(n)}_{2,\pm}}}\end{pmatrix}\right]^{\mathrm{T}}\widehat{T}_l\Psi^{\pm}(\vec{r}_m),\end{aligned} \tag{11}$$

where $t_{1;l,a_m}$ and $t_{2;l,a_m}$ are scattering coefficients for the mth scatterer, $\widehat{T}_l$ is a scattering operator defined in appendix A, $l_{\max}$ is the largest harmonic used in the multiple scattering calculations, and δ_{ij} is the Kronecker delta: $\delta_{ij} = 0$ for $i \neq j$ and $\delta_{ij} = 1$ for $i = j$.

Similarly, for $x \ll -d$, the total wave function can be written as a sum of the incident and reflected wave functions overall all open channels, $\Psi^{\pm}(\vec{r}) = \phi^{\pm}_{\vec{k}_\pm}(\vec{r}) + \Psi^{\pm}_{\mathscr{R}}(\vec{r})$, where the reflected wave function is given by:

$$\Psi^{\pm}_{\mathscr{R}}(\vec{r}) = \sum_{n\in\mathscr{N}_{1,\pm}} \mathscr{R}^{(n)}_{1,\pm}\phi^{+}_{\overline{\vec{k}^{(n)}}_{1,\pm}}(\vec{r}) + \sum_{p\in\mathscr{N}_{2,\pm}} \mathscr{R}^{(p)}_{2,\pm}\phi^{-}_{\overline{\vec{k}^{(p)}}_{2,\pm}}(\vec{r}), \tag{12}$$

where $\overline{\vec{k}^{(n)}}_{b,\pm} = k^{(n)}_{bY,\pm}\hat{y} - k^{(n)}_{bX,\pm}\hat{x}$, and

$$\begin{aligned}\mathscr{R}^{(n)}_{1,\pm} &= \sum_{m=1}^{N_s}\sum_{l=-l_{\max}}^{l_{\max}} \frac{(-1)^l t_{1;l,a_m}\mathrm{e}^{-\mathrm{i}\,\overline{\vec{k}^{(p)}}_{1,\pm}\cdot\vec{r}_m}}{d} \\ &\quad\times\sqrt{\frac{2\hbar\overline{k}}{m^* k_1 k^{(n)}_{1X,\pm}}}\left[\begin{pmatrix}\mathrm{e}^{\mathrm{i}l\theta_{\bar{k}^{(n)}_{1,\pm}}} \\ -\mathrm{i}\mathrm{e}^{-\mathrm{i}(l-1)\theta_{\bar{k}^{(n)}_{1,\pm}}}\end{pmatrix}\right]^{\mathrm{T}}\widehat{T}_l\Psi^{\pm}(\vec{r}_m) \\ \mathscr{R}^{(n)}_{2,\pm} &= \sum_{m=1}^{N_s}\sum_{l=-l_{\max}}^{l_{\max}} \frac{(-1)^l t_{2;l,a_m}\mathrm{e}^{-\mathrm{i}\,\overline{\vec{k}^{(n)}}_{2,\pm}\cdot\vec{r}_m}}{d} \\ &\quad\times\sqrt{\frac{2\hbar\overline{k}}{m^* k_2 k^{(n)}_{2X,\pm}}}\left[\begin{pmatrix}\mathrm{e}^{\mathrm{i}l\theta_{\bar{k}^{(n)}_{2,\pm}}} \\ \mathrm{i}\mathrm{e}^{-\mathrm{i}(l-1)\theta_{\bar{k}^{(n)}_{2,\pm}}}\end{pmatrix}\right]^{\mathrm{T}}\widehat{T}_l\Psi^{\pm}(\vec{r}_m).\end{aligned} \tag{13}$$

The total spin-resolved transmission and reflection probabilities, which are given by $\mathscr{T}_{b,\pm} = \sum_{n\in\mathscr{N}_{b,\pm}}|\mathscr{T}^{(n)}_{b,\pm}|^2$ and $\mathscr{R}_{b,\pm} = \sum_{n\in\mathscr{N}_{b,\pm}}|\mathscr{R}^{(n)}_{b,\pm}|^2$ for $b = 1$ and $b = 2$, respectively, satisfy the unitarity condition imposed by flux conservation:

$$\mathscr{T}_{1,\pm} + \mathscr{T}_{2,\pm} + \mathscr{R}_{1,\pm} + \mathscr{R}_{2,\pm} = 1. \tag{14}$$

In figure 2(B), the calculated total spin subband resolved transmission ($\mathscr{T}_{1,\pm}$ and $\mathscr{T}_{2,\pm}$) and reflection ($\mathscr{R}_{1,\pm}$ and $\mathscr{R}_{2,\pm}$) probabilities are shown as a function of $\frac{d}{\overline{\lambda}} = \frac{\overline{k}d}{2\pi}$ and angle of incidence, θ_0, for a plane-wave in the '±'-spin subband (equation (3)) that is scattered by a quasi-one-dimensional scattering array [$d = 300$ nm]. In the calculations, the scattering array's unit cell consisted of a single scatterer with $a_1 = 40$ nm and $V_1 = -0.2$ eV. Generally, as $\frac{d}{\overline{\lambda}}$ increased, transmission for normally incident waves ($\theta_0 \approx 0$) increased, independent of spin subband. In figure 2(B), $\mathscr{T}_{1(2),\pm}$ and $\mathscr{R}_{1(2),\pm}$ were either enhanced or depressed along curves representing threshold conditions [28] where additional open channels become available, i.e. where either $k^{(n)}_{1X,\pm} = 0$ and/or $k^{(n)}_{2X,\pm} = 0$ These threshold conditions are given in terms of $0 \leqslant \theta_0 < \frac{\pi}{2}$ and $\frac{d}{\overline{\lambda}} \geqslant \frac{d}{\lambda_\alpha}$ by:

$$\frac{d}{\overline{\lambda}} = \begin{cases} \frac{n}{1-\sin(|\theta_0|)} - \frac{d}{\lambda_\alpha} & \text{for } n \geqslant \left[\frac{2d}{\lambda_\alpha}\right]_+ \text{ and } 0 \leqslant |\theta_0| < \frac{\pi}{2} \\ \frac{n}{1-\sin(|\theta_0|)} - \frac{d}{\lambda_\alpha} & \text{for } 0 < n < \left[\frac{2d}{\lambda_\alpha}\right]_+ \text{ and } \sin^{-1}\left(1 - \frac{\lambda_\alpha}{2d}n\right) \leqslant |\theta_0| \leqslant \frac{\pi}{2} \\ \frac{|n|}{1+\sin(|\theta_0|)} - \frac{d}{\lambda_\alpha} & \text{for } -\left[\frac{4d}{\lambda_\alpha}\right]_+ < n \leqslant -\left[\frac{2d}{\lambda_\alpha}\right]_+ < 0 \text{ and } 0 \leqslant |\theta_0| \leqslant \sin^{-1}\left(\frac{\lambda_\alpha}{2d}|n| - 1\right) \\ \frac{|n|}{1+\sin(|\theta_0|)} - \frac{d}{\lambda_\alpha} & \text{for } n \leqslant -\left[\frac{4d}{\lambda_\alpha}\right]_+ < 0 \text{ and } 0 \leqslant |\theta_0| < \frac{\pi}{2} \end{cases} \tag{15}$$

$$\frac{d}{\overline{\lambda}} = \begin{cases} \frac{\frac{d}{\lambda_\alpha}(1+\sin(|\theta_0|))+n}{1-\sin(|\theta_0|)} & \text{for } n \geqslant 0 \text{ and } 0 \leqslant |\theta_0| \leqslant \frac{\pi}{2} \\ \frac{\frac{d}{\lambda_\alpha}(1-\sin(|\theta_0|))+|n|}{1+\sin(|\theta_0|)} & \text{for } 0 > n > -\left[\frac{2d}{\lambda_\alpha}\right]_+ \text{ and } 0 \leqslant |\theta_0| < \sin^{-1}\left(\frac{\lambda_\alpha|n|}{2d}\right) \\ \frac{\frac{d}{\lambda_\alpha}(1-\sin(|\theta_0|))+|n|}{1+\sin(|\theta_0|)} & \text{for } n \leqslant -\left[\frac{2d}{\lambda_\alpha}\right]_+ < 0 \text{ and } 0 \leqslant |\theta_0| < \frac{\pi}{2} \end{cases} \tag{16}$$

for $\mathscr{T}_{1,+}/\mathscr{R}_{1,+}$ and $\mathscr{T}_{2,+}/\mathscr{R}_{2,+}$, respectively, and

$$\frac{d}{\overline{\lambda}} = \begin{cases} \frac{n - \frac{d}{\lambda_\alpha}(1+|\sin(\theta_0)|)}{1-|\sin(\theta_0)|} & \text{for } n \geqslant \left[\frac{2d}{\lambda_\alpha}\right]_+ \text{ and } 0 \leqslant |\theta_0| < \frac{\pi}{2} \\ \frac{\left|n\right| - \frac{d}{\lambda_\alpha}(1-|\sin(\theta_0)|)}{1+|\sin(\theta_0)|} & \text{for } n \leqslant -\left[\frac{2d}{\lambda_\alpha}\right]_+ \text{ and } 0 \leqslant |\theta_0| < \frac{\pi}{2} \end{cases} \tag{17}$$

$$\frac{d}{\overline{\lambda}} = \begin{cases} \frac{d}{\lambda_\alpha} + \frac{n}{1-|\sin(\theta_0)|} & \text{for } n \geqslant 0 \text{ and } 0 \leqslant |\theta_0| < \frac{\pi}{2} \\ \frac{d}{\lambda_\alpha} + \frac{|n|}{1+|\sin(\theta_0)|} & \text{for } n \leqslant -1 \text{ and } 0 \leqslant |\theta_0| < \frac{\pi}{2} \end{cases} \tag{18}$$

for $\mathscr{T}_{1,-}/\mathscr{R}_{1,-}$ and $\mathscr{T}_{2,-}/\mathscr{R}_{2,-}$, respectively. Note again that since $k_{1X,\pm}^{(0)} \geqslant 0$ for $\overline{\lambda} \geqslant \lambda_\alpha$, there is always at least one open channel in the '+'-spin subband for an arbitrary incident wave. In figure 2(B), there are regions of $\frac{d}{\lambda_\alpha} \leqslant \frac{d}{\overline{\lambda}} \leqslant \frac{d}{\lambda_\alpha} + \frac{1}{2}$ and θ_0 bounded by the curves given in equation (8) (with $\Theta_{\text{inter}} = \frac{\pi}{8.456}$ for the parameters used in figure 2(B)) where $\mathscr{T}_{2,+} = \mathscr{R}_{2,+} = 0$ due to the fact that $\mathscr{N}_{2,-} = \{\varnothing\}$.

2.2. The probability density for the transmitted wave function

The corresponding (dimensionless) probability and polarization density for $x \gg d$ can be written as:

$$\frac{\hbar\overline{k}}{m^*}\Psi_{\mathscr{T}}^{\pm}(\vec{r})(\Psi_{\mathscr{T}}^{\pm}(\vec{r}))^\dagger = \rho_{\mathscr{T}}^{\pm}(\vec{r})\hat{1} + \vec{P}_{\mathscr{T},\vec{\sigma}}^{\pm}(\vec{r}) \cdot \vec{\sigma}, \tag{19}$$

where $\rho_{\mathscr{T}}^{\pm}(\vec{r})$ and $\vec{P}_{\mathscr{T},\vec{\sigma}}^{\pm}(\vec{r}) = P_{\mathscr{T},\hat{\sigma}_X}^{\pm}(\vec{r})\hat{x} + P_{\mathscr{T},\hat{\sigma}_Y}^{\pm}(\vec{r})\hat{y} + P_{\mathscr{T},\hat{\sigma}_Z}^{\pm}(\vec{r})\hat{z}$ are the probability and spin vector polarization densities for the transmitted wave function, respectively, $\hat{1}$ is a 2×2 identity matrix, and $\vec{\sigma} = (\hat{\sigma}_X, \hat{\sigma}_Y, \hat{\sigma}_Z)$ is a vector of Paul spin matrices. Expressions for $\vec{P}_{\mathscr{T},\vec{\sigma}}^{\pm}(\vec{r})$, the reflected probability density, $\rho_{\mathscr{R}}^{\pm}(\vec{r})$, and the reflected spin vector polarization densities, $\vec{P}_{\mathscr{R},\vec{\sigma}}^{\pm}(\vec{r})$, are given in appendix C.

Using equation (10) and writing the transmission coefficient for the nth open channel as $\mathscr{T}_{1,\pm}^{(n)} = |\mathscr{T}_{1,\pm}^{(n)}| \exp\left(i\left(\theta_{\mathscr{T}_{1,\pm}^{(n)}} - \frac{\theta_{\vec{k}_{1,\pm}^{(n)}}}{2}\right)\right)$ for $n \in \mathscr{N}_{1,\pm}$ and $\mathscr{T}_{2,\pm}^{(m)} = |\mathscr{T}_{2,\pm}^{(m)}| \exp\left(i\left(\theta_{\mathscr{T}_{2,\pm}^{(m)}} - \frac{\theta_{\vec{k}_{2,\pm}^{(m)}}}{2}\right)\right)$ for $m \in \mathscr{N}_{2,\pm}$, $\rho_{\mathscr{T}}^{\pm}(\vec{r})$ can be written as:

$$\begin{aligned} \rho_{\mathscr{T}}^{\pm}(\vec{r}) &= \rho_{\mathscr{T},11}^{\pm}(\vec{r}) + \rho_{\mathscr{T},22}^{\pm}(\vec{r}) + \rho_{\mathscr{T},12}^{\pm}(\vec{r}) \\ &= \rho_{\mathscr{T},\text{intra}}^{\pm}(\vec{r}) + \rho_{\mathscr{T},12}^{\pm}(\vec{r}) \end{aligned} \tag{20}$$

with

$$\begin{aligned} \rho_{\mathscr{T},bb}^{\pm}(\vec{r}) = \sum_{n\in\mathscr{N}_{b,\pm}} \sum_{m\in\mathscr{N}_{b,\pm}} & \frac{k_b|\mathscr{T}_{b,\pm}^{(n)}\mathscr{T}_{b,\pm}^{(m)}|\cos(\phi_{b,b,\pm}^{(n,m)})}{2\sqrt{k_{bX,\pm}^{(n)}k_{bX,\pm}^{(m)}}} \\ & \times \exp(i[(\vec{k}_{b,\pm}^{(n)} - \vec{k}_{b,\pm}^{(m)}) \cdot \vec{r} + \Delta\theta_{\mathscr{T}_{b,b,\pm}^{(n,m)}}]) \end{aligned} \tag{21}$$

$$\begin{aligned} \rho_{\mathscr{T},12}^{\pm}(\vec{r}) = \sum_{n\in\mathscr{N}_{1,\pm}} \sum_{m\in\mathscr{N}_{2,\pm}} & \frac{\sqrt{k_1k_2}|\mathscr{T}_{1,\pm}^{(n)}\mathscr{T}_{2,\pm}^{(m)}|\sin(\phi_{1,2,\pm}^{(n,m)})}{\sqrt{k_{1X,\pm}^{(n)}k_{2X,\pm}^{(m)}}} \\ & \times \sin((\vec{k}_{1,\pm}^{(n)} - \vec{k}_{2,\pm}^{(m)}) \cdot \vec{r} + \Delta\theta_{\mathscr{T}_{1,2,\pm}^{(n,m)}}), \end{aligned} \tag{22}$$

where the phase shifts $\Delta\theta_{\mathscr{T}_{a,b,\pm}^{(m,n)}} = \theta_{\mathscr{T}_{a,\pm}^{(m)}} - \theta_{\mathscr{T}_{b,\pm}^{(n)}}$ are a result of the Talbot–Beeby effect [29], and the $\cos(\phi_{b,b,\pm}^{(m,n)})$ and $\sin(\phi_{1,2,\pm}^{(m,n)})$ amplitude factors in equations (21) and (22) with $\phi_{a,b,\pm}^{(m,n)} = \frac{\theta_{\vec{k}_{a,\pm}^{(m)}} - \theta_{\vec{k}_{b,\pm}^{(n)}}}{2}$ are the result of the spinor nature of plane-wave states in equation (3). The above phase shifts and amplitude factors are due to the spinor nature of the plane-wave eigenstates of $\widehat{H}_0$ in equation (3) and are similar to prior theoretical predictions for quasiparticle scattering in monolayer graphene [16].

The contributions to $\rho_{\mathscr{T}}^{\pm}(\vec{r})$ in equation (20) arising from interference between open channels within the same spin subband, $\rho_{\mathscr{T},11}^{\pm}(\vec{r})$ and $\rho_{\mathscr{T},22}^{\pm}(\vec{r})$, are given in equation (21).

Defining the wavelengths $\lambda_1 = \frac{2\pi}{k_1}$ and $\lambda_2 = \frac{2\pi}{k_2}$, the conditions for there to be *intraspin* subband interference are that $\mathscr{N}_{1,\pm}$ and/or $\mathscr{N}_{2,\pm}$ contain at least two open channels. For an incident wave in the '+'-spin subband, $\mathscr{N}_{1,+}$ will contain at least two elements when:

$$\frac{d}{\lambda_1} > \frac{1}{1 + |\sin(\theta_0)|} \tag{23}$$

which will always be satisfied when $\frac{d}{\lambda_1} > 1$.

For $\mathscr{N}_{2,+}$ to contain at least two elements with $\frac{d}{\lambda_2} > 0$ requires that $\frac{d}{\lambda_2} > 1 - \frac{d}{\lambda_1}|\sin(\theta_0)|$ when $\frac{1}{2} \geqslant \frac{d}{\lambda_1}$ or that $\frac{d}{\lambda_2} > 1 - \frac{d}{\lambda_1}|\sin(\theta_0)|$ for $0 \leqslant |\theta_0| \leqslant \sin^{-1}\left(\frac{\lambda_1}{2d}\right)$ and $\frac{d}{\lambda_2} > \frac{d}{\lambda_1}|\sin(\theta_0)|$ for $\sin^{-1}\left(\frac{d}{2\lambda_1}\right) \leqslant |\theta_0|$ when $\frac{1}{2} < \frac{d}{\lambda_1} \leqslant 1$. When $1 < \frac{d}{\lambda_1}$, $\mathscr{N}_{2,+}$ will contain at least two elements when:

$$\frac{d}{\lambda_2} > \begin{cases} 1 - \frac{d}{\lambda_1}|\sin(\theta_0)| & 0 \leqslant |\theta_0| \leqslant \sin^{-1}\left(\frac{\lambda_1}{2d}\right) \\ \frac{d}{\lambda_1}|\sin(\theta_0)| & \sin^{-1}\left(\frac{\lambda_1}{2d}\right) \leqslant |\theta_0| \leqslant \sin^{-1}\left(\frac{\lambda_1}{d}\right) \\ 2 - \frac{d}{\lambda_1}|\sin(\theta_0)| & \text{for } \sin^{-1}\left(\frac{\lambda_1}{d}\right) \leqslant |\theta_0| \end{cases} \tag{24}$$

For an incident wave in the '−'-spin subband, $\mathscr{N}_{2,-}$ will contain at least two elements when:

$$\frac{d}{\lambda_2} > \frac{1}{1 + |\sin(\theta_0)|} \text{ for } 0 \leqslant |\theta_0| < \frac{\pi}{2} \tag{25}$$

$\mathscr{N}_{1,-}$ will also contain at least two elements when:

$$\frac{d}{\lambda_1} > 1 - \frac{d}{\lambda_2}|\sin(\theta_0)| \text{ for } 0 \leqslant |\theta_0| < \frac{\pi}{2}. \tag{26}$$

Equations (23)–(26) summarize the conditions for the occurrence of *intraspin* subband interference.

The other contribution to $\rho^{\pm}_{\mathscr{F}}(\vec{r})$, $\rho^{\pm}_{\mathscr{F},12}(\vec{r})$ in equation (22), arises from *interspin* subband interference. For an incident wave in the '−'-spin subband with $|\vec{k}_{\text{inc.}}| = |k_-| = k_2$, interference between open channels in different spin subbands exists for all θ_0 and for all $\frac{d}{\lambda_1} > \frac{2d}{\lambda_\alpha}$ and $\frac{d}{\lambda_2} > 0$. However, for an incident wave in the '+'-spin subband with $|\vec{k}_{\text{inc.}}| = |k_+| = k_1$, interference between open channels in different spin subbands requires that $\mathscr{N}_{2,+} \neq \{\varnothing\}$ and will occur when $\frac{d}{\lambda_1} > \frac{1}{2}$ for θ_0 satisfying:

$$\frac{d}{\lambda_2} > \begin{cases} \frac{d}{\lambda_1}|\sin(\theta_0)| & 0 \leqslant |\theta_0| \leqslant \sin^{-1}\left(\frac{\lambda_1}{2d}\right) \\ 1 - \frac{d}{\lambda_1}|\sin(\theta_0)| & \sin^{-1}\left(\frac{\lambda_1}{2d}\right) \leqslant |\theta_0| \end{cases} \tag{27}$$

For $\frac{d}{\lambda_1} \leqslant \frac{1}{2}$, a necessary condition for *interspin* subband interference is that $\frac{d}{\lambda_2} > \frac{d}{\lambda_1}|\sin(\theta_0)|$ for all θ_0. As will be discussed below, *interspin* subband interference generates an additional Talbot length that is inversely proportional to the spin–orbit coupling constant, α.

3. The Talbot effect

In equation (20), $\rho^{\pm}_{\mathscr{F}}(\vec{r})$ is periodic along the $\hat{y}$-direction with periods $\left|\frac{d}{m-n}\right|$ for $m \neq n$. Additionally, $\rho^{\pm}_{\mathscr{F}}(\vec{r})$ is also periodic along the $\hat{x}$-direction with periods given by $\left|\frac{2\pi}{k^{(m)}_{1X,\pm} - k^{(n)}_{1X,\pm}}\right|$ and $\left|\frac{2\pi}{k^{(m)}_{2X,\pm} - k^{(n)}_{2X,\pm}}\right|$ for $m \neq n$ due to *intraspin* subband interference and $\left|\frac{2\pi}{k^{(m)}_{1X,\pm} - k^{(n)}_{2X,\pm}}\right|$ due to *interspin* subband interference. The periodicity along the $\hat{x}$-direction and the corresponding contributions from *interspin* and *intraspin* subband scattering can be readily found by applying a Fourier transformation along the $\hat{x}$ direction to either $\rho^{\pm}_{\mathscr{F}}(\vec{r})$ or $\rho^{\pm}_{\mathscr{F},\text{intra}}(\vec{r})$ for $-\frac{d}{2} \leqslant y \leqslant \frac{d}{2}$:

$$\begin{aligned} \tilde{\rho}^{\pm}_{\mathscr{F}}(y, k_X) &= \left| \int_0^\infty \mathrm{d}x \rho^{\pm}_{\mathscr{F}}(y\hat{y} + x\hat{x}) \mathrm{e}^{-\mathrm{i}k_X x} \right| \\ \tilde{\rho}^{\pm}_{\mathscr{F},\text{intra}}(y, k_X) &= \left| \int_0^\infty \mathrm{d}x \rho^{\pm}_{\mathscr{F},\text{intra}}(y\hat{y} + x\hat{x}) \mathrm{e}^{-\mathrm{i}k_X x} \right|. \end{aligned} \tag{28}$$

In this case, $\tilde{\rho}^{\pm}_{\mathscr{F},\text{intra}}(y, k_X)$ represents a 'power spectrum' with peaks occurring at values of k_X that are inversely proportional to one of the *intraspin* subband Talbot lengths, $z^{(m,n)}_{\text{Talbot},11,\pm}$ and $z^{(m,n)}_{\text{Talbot},22,\pm}$, while $\tilde{\rho}^{\pm}_{\mathscr{F}}(y, k_X)$ is a 'power spectrum' with additional peaks that are inversely proportional to the *interspin* subband Talbot lengths, $z^{(m,n)}_{\text{Talbot},12,\pm}$.

For $|m| > |n| \geqslant 0$ with $m, n \in \mathscr{N}_{1,\pm}$ or $m, n \in \mathscr{N}_{2,\pm}$, the *intraspin* subband Talbot lengths are given by:

$$\begin{aligned} z^{(m,n)}_{\text{Talbot},bb,\pm} &= \frac{2\pi}{k^{(n)}_{bX,\pm} - k^{(m)}_{bX,\pm}} \\ &= \frac{\lambda_b}{\sqrt{1 - \left(\frac{\lambda_b}{\lambda_\pm}\sin(\theta_0) + \frac{n\lambda_b}{d}\right)^2} - \sqrt{1 - \left(\frac{\lambda_b}{\lambda_\pm}\sin(\theta_0) + \frac{m\lambda_b}{d}\right)^2}}, \end{aligned} \tag{29}$$

where either $b = 1$ (for $z^{(m,n)}_{\text{Talbot},11,\pm}$) or $b = 2$ (for $z^{(m,n)}_{\text{Talbot},22,\pm}$), and $\lambda_+ = \lambda_1$ and $\lambda_- = \lambda_2$. For a normally incident wave ($\theta_0 = 0$), the Talbot lengths are independent of the spin subband of the incident wave. Furthermore, when either $\lambda_1 \ll d$ and/or $\lambda_2 \ll d$, the paraxial approximation can be made such that $z^{(m,n)}_{\text{Talbot},11,\pm} \approx \frac{2d^2}{(m^2 - n^2)\lambda_1}$ and $z^{(m,n)}_{\text{Talbot},22,\pm} \approx \frac{2d^2}{(m^2 - n^2)\lambda_2}$, with the traditional Talbot distances defined by Lord Rayleigh [7] corresponding to $z_{1\text{T}} \equiv z^{(1,0)}_{\text{Talbot},11,\pm} \approx \frac{2d^2}{\lambda_1} = \frac{\lambda_2}{\lambda_1} z^{(1,0)}_{\text{Talbot},22,\pm} = \frac{\lambda_2}{\lambda_1} z_{2\text{T}}$. The generation of two distinct *intraspin* subband Talbot lengths, $z_{1\text{T}}$ and $z_{2\text{T}}$, from an incident wave is a unique feature that arises due to spin–orbit coupling. The relative difference in these Talbot lengths, χ, can be written as:

$$\chi = \frac{z_{1\text{T}} - z_{2\text{T}}}{z_{1\text{T}} + z_{2\text{T}}} = \frac{m^*\alpha}{\hbar^2\sqrt{\frac{2m^*E}{\hbar^2} + \left(\frac{m^*\alpha}{\hbar^2}\right)^2}} = \frac{\overline{\lambda}}{\lambda_\alpha} \tag{30}$$

which decreases as $E^{-\frac{1}{2}}$.

The other Talbot length due to *interspin* subband interference, $z^{(m,n)}_{\text{Talbot},12,\pm}$, is given:

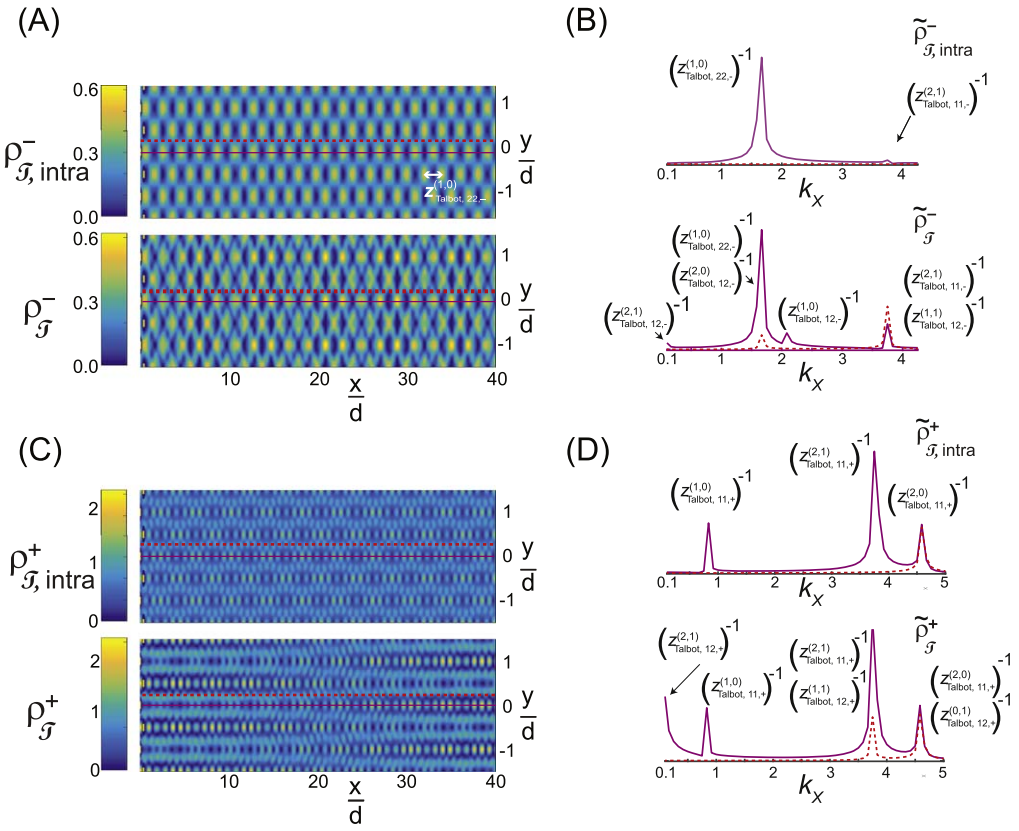

Figure 3. Plots of $\rho^{\pm}_{\mathcal{I},\text{intra}}(\vec{r})$ (equation (21)) and $\rho^{\pm}_{\mathcal{I}}(\vec{r})$ (equation (20)) for a plane-wave in either (A) the '−'-spin subband or (C) the '+'-spin subband with $\frac{kd}{2\pi} = 1.7$ that is normally incident ($\theta_0 = 0$) to a periodic scattering array with $d = 300$ nm and with a unit cell consisting of $N_s = 2$ identical scatterers with $a_1 = a_2 = 60$ nm, $V_1 = V_2 = 0.1$ eV, $\vec{r}_1 = 0$, and $\frac{\vec{r}_2}{\text{nm}} = 120\hat{x} + 150\hat{y}$. In (B) and (D), the corresponding 'power spectra', $\tilde{\rho}^{\pm}_{\mathcal{I}}(y, k_X)$ and $\tilde{\rho}^{\pm}_{\mathcal{I},\text{intra}}(y, k_X)$ from equation (28) at (magenta) $y = 0$ and (red dashed) $y = 0.25d$, are shown with the relevant Talbot lengths labeled. The open channels were given by $\mathcal{N}_{1,+} = \mathcal{N}_{1,-} = \{0, \pm 1, \pm 2\}$ and $\mathcal{N}_{2,+} = \mathcal{N}_{2,-} = \{0, \pm 1\}$. For an incident wave in the '−'-spin subband (figure 3(A)), $\mathcal{T}_{1,-} = 0.0272$ and $\mathcal{T}_{2,-} = 0.1538$ while for an incident wave in the '+'-spin subband (figure 3(C)), $\mathcal{T}_{1,+} = 0.2335$ and $\mathcal{T}_{2,+} = 0.1638$. It can be seen by comparing $\rho^{\pm}_{\mathcal{I},\text{intra}}(\vec{r})$ to $\rho^{\pm}_{\mathcal{I}}(\vec{r})$ that *interspin* subband interference results in significant changes to the shape and intensities of the interference patterns in $\rho_{\mathcal{I}^{\pm}}(\vec{r})$, which is also reflected in the changes in the 'power spectra' shown in (B) and (D).

$$z^{(m,n)}_{\text{Talbot},12,\pm} = \left| \frac{\lambda_1}{\sqrt{1 - \left(\frac{\lambda_1}{\lambda_\pm}\sin(\theta_0) + \frac{\lambda_1 m}{d}\right)^2} - \frac{\lambda_1}{\lambda_2}\sqrt{1 - \left(\frac{\lambda_2}{\lambda_\pm}\sin(\theta_0) + \frac{\lambda_2 n}{d}\right)^2}} \right|, \tag{31}$$

where in general, $z^{(m,n)}_{\text{Talbot},12,\pm} \neq z^{(n,m)}_{\text{Talbot},12,\pm}$. For a normally incident beam, $z^{(m,n)}_{\text{Talbot},12,\pm}$ is again independent of the spin subband of the incident wave. In the paraxial approximation, $z^{(m,n)}_{\text{Talbot},12,\pm}$ is given by:

$$z^{(m,n)}_{\text{Talbot},12,\pm} \approx \left| \frac{\lambda_1\lambda_2}{(\lambda_2 - \lambda_1)\left(1 + \frac{\lambda_1\lambda_2(n^2 - m^2)}{2d^2}\right)} \right| \approx \frac{\lambda_\alpha}{2}\left| 1 - \frac{\lambda_1\lambda_2(n^2 - m^2)}{2d^2} \right|. \tag{32}$$

When $d \gg \lambda_1$ and $d \gg \lambda_2$, an analogous Talbot distance for interference between different spin subbands can be written as $z_{12\text{T}} = z^{(m,n)}_{\text{Talbot},12,\pm} \approx \frac{\lambda_\alpha}{2}$, which is independent of d. Note that while $z^{(0,0)}_{\text{Talbot},12,\pm} \approx \frac{\lambda_\alpha}{2} \neq 0$ at normal incidence, the $n = 0$ open channels in $\mathcal{N}_{1,\pm}$ and $\mathcal{N}_{2,\pm}$ are orthogonal to one another, i.e. $(\phi^{+}_{\vec{k}_{1,\pm}^{(0)}}(\vec{r}))^{\dagger}\phi^{-}_{\vec{k}_{2,\pm}^{(0)}}(\vec{r}) = 0$, which means no *interspin* subband interference between the $n = 0$ open channels in $\mathcal{N}_{1,\pm}$ and $\mathcal{N}_{2,\pm}$ can occur at normal incidence.

An illustration of the contributions from *intraspin* and *interspin* subband interference to $\rho_{\mathcal{I}^{\pm}}(\vec{r})$ are shown in figure 3

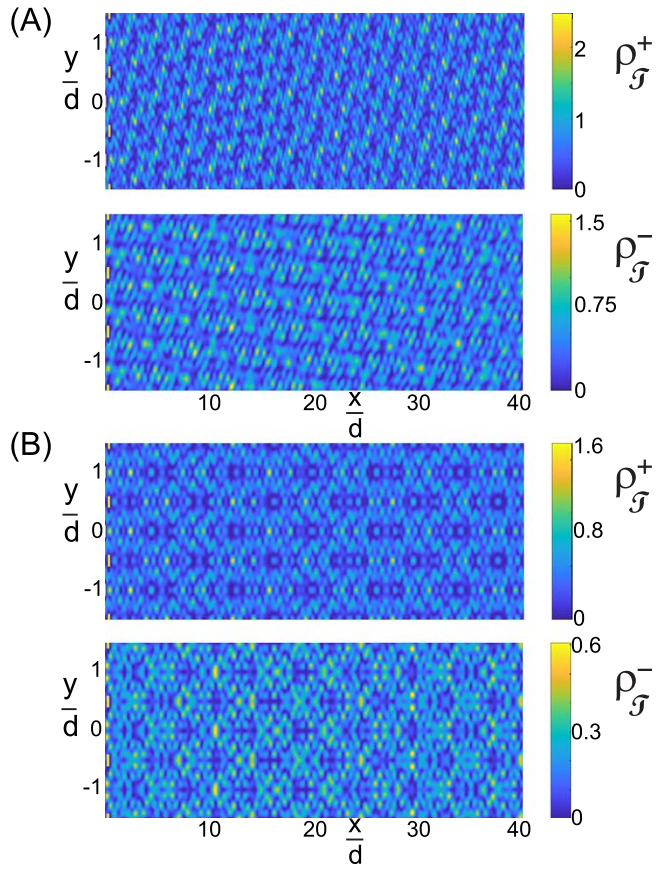

Figure 4. Plots of $\rho^{\pm}_{\mathscr{T}}(\vec{r})$ (equation (20)) for a corresponding plane-wave in the '±'-spin subband with $\frac{kd}{2\pi} = 3.2$ that is incident to the same scattering array used in figure 3 but at an angle of incidence of either (A) $\theta_0 = \frac{\pi}{4}$ or (B) $\theta_0 = 0$. (A) For an incident wave in the '+'-spin subband, $\mathscr{N}_{1,+} = \{-6,\cdots,1\}$, $\mathscr{N}_{2,+} = \{-4,\cdots,0\}$ with $T_{1,+} = 0.2911$ and $T_{2,+} = 0.1545$, while for an incident wave in the '−'-spin subband, $\mathscr{N}_{1,-} = \{-5,\cdots,1\}$, $\mathscr{N}_{2,-} = \{-4,\cdots,0\}$ with $T_{1,+} = 0.1765$ and $T_{2,-} = 0.1563$. (B) For an incident waves in the '±'-spin subbands, $\mathscr{N}_{1,+} = \mathscr{N}_{1,-} = \{0, \pm1, \pm2, \pm3\}$ and $\mathscr{N}_{2,+} = \mathscr{N}_{2,-} = \{0, \pm1, \pm2\}$, but with $T_{1,+} = 0.2063$ and $T_{2,+} = 0.1014$ and with $T_{1,+} = 0.0737$ and $T_{2,-} = 0.0743$.

by plotting the calculated contributions from *intraspin* subband interfence, $\rho^{\pm}_{\mathscr{T},\text{intra}}(\vec{r})$, and the calculated contributions from both *intraspin* and *interspin* subband interference, $\rho^{\pm}_{\mathscr{T}}(\vec{r})$, for an incident wave in either the (figure 3(A)) '−'-spin subband or in the (figure 3(C)) '+'-spin subband. In all cases, $\Psi^{\pm}_{\mathscr{T}}(\vec{r})$ (equation (10)) was calculated using only 'open' channels, which for the parameters used in figure 3 [$\frac{d}{\lambda} = 1.7$ and $\frac{d}{\lambda_\alpha} = 0.438\,619$], resulted in $\mathscr{N}_{1,+} = \mathscr{N}_{1,-} = \{0, \pm1, \pm2\}$ and $\mathscr{N}_{2,+} = \mathscr{N}_{2,-} = \{0, \pm1\}$. In addition, the corresponding $\widetilde{\rho}^{\pm}_{\mathscr{T}}(y, k_X)$ in equation (28) were also numerically evaluated at (magenta line) $\frac{y}{d} = 0$ and (red dashed line) $\frac{y}{d} = 0.25$, with a resolution in k_X being $\Delta k_X = 1/12000\,\text{nm}^{-1}$. In figure 3(A), one dominant *intraspin* Talbot length was observed, $z^{(1,0)}_{\text{Talbot},22,-} = 609.06$ nm (which is also shown in figure 3(A)), with another Talbot length, $z^{(2,1)}_{\text{Talbot},11,-} = 264.78$ nm also visible in $\widetilde{\rho}^{-}_{\mathscr{T},\text{intra}}(0, k_X)$ in figure 3(B). The *intraspin* Talbot lengths $z^{(2,0)}_{\text{Talbot},11,-} = 217.20$ nm and $z^{(1,0)}_{\text{Talbot},11,-} = 1.208\,7 \times 10^3$ nm were not observed since $\mathscr{T}^{(0)}_{1,-} = 0$. Note that at $y = 0.25d$, $\rho^{-}_{\mathscr{T},\text{intra}}(\vec{r})$ is constant and hence the absence of any peaks in $\widetilde{\rho}^{\pm}_{\mathscr{T},\text{intra}}(0.25d, k_X)$ in figure 3(B). When considering the contributions from *interspin* subband interference, four *interspin* Talbot lengths were also observed, $z^{(2,0)}_{\text{Talbot},12,-} = 595.29$ nm, $z^{(1,0)}_{\text{Talbot},12,-} = 476.92$ nm, $z^{(2,1)}_{\text{Talbot},12,-} = 2.632\,82 \times 10^4$ nm, and $z^{(1,1)}_{\text{Talbot},12,-} = 267.47$ nm. Note that while all *interspin* Talbot lengths contributed to $\widetilde{\rho}^{-}_{\mathscr{T}}(0, k_X)$, only $z^{(2,0)}_{\text{Talbot},12,-}$ and $z^{(1,1)}_{\text{Talbot},12-}$ contributed to $\widetilde{\rho}^{-}_{\mathscr{T}}(0.25d, k_X)$. In figure 3(C), three *intraspin* Talbot lengths $z^{(2,1)}_{\text{Talbot},11,+} = 264.78$ nm, $z^{(2,0)}_{\text{Talbot},11,+} = 217.20$ nm, and $z^{(1,0)}_{\text{Talbot},11,+} = 1.208\,7 \times 10^3$ nm were observed while $z^{(1,0)}_{\text{Talbot},22,+} = 609.06$ nm was not observed since $\mathscr{T}^{(0)}_{2,+} = 0$. Note also that only $z^{(2,0)}_{\text{Talbot},11,+}$ contributed to $\widetilde{\rho}^{+}_{\mathscr{T},\text{intra}}(0.25d, k_X)$. Three *interspin* Talbot lengths $z^{(0,1)}_{\text{Talbot},12,+} = 219.01$ nm, $z^{(1,1)}_{\text{Talbot},12,+} = 267.47$ nm, and $z^{(2,1)}_{\text{Talbot},12,+} = 2.632\,82 \times 10^4$ nm were also observed, where only $z^{(1,1)}_{\text{Talbot},12,+}$ (along with $z^{(2,0)}_{\text{Talbot},11,+}$) contributed to $\widetilde{\rho}^{+}_{\mathscr{T}}(0.25d, k_X)$ in figure 3(D). In both figures 3(A) and (C), *interspin* subband interference noticably affected the shape of the interference patterns in $\rho_{\mathscr{T}^{\pm}}(\vec{r})$.

In figure 4, calculations of $\rho^{\pm}_{\mathscr{T}}(\vec{r})$ are shown for waves in the '±'-spin subband with $\frac{d}{\lambda} = 3.2$ that were incident to the same scattering array used in figure 3 but at incidence angles of either (figure 4(A)) $\theta_0 = \frac{\pi}{4}$ or (figure 4(B)) $\theta_0 = 0$. For $\theta_0 = \frac{\pi}{4}$ (figure 4(A)), a clearly defined 'slant' in $\rho^{\pm}_{\mathscr{T}}(\vec{r})$ was observed, which is related to the fact the open channels indices, n, are not symmetric about $n = 0$: $\mathscr{N}_{1,+} = \{-6,\cdots,1\}$, $\mathscr{N}_{2,+} = \{-4,\cdots,0\}$, $\mathscr{N}_{1,-} = \{-5,\cdots,1\}$ and $\mathscr{N}_{2,-} = \{-4,\cdots,0\}$. At normal incidence (figure 4(B)), periodic modulations in $\rho^{\pm}_{\mathscr{T}}(\vec{r})$ were again symmetric about the $\hat{x}$-direction, similar to those shown in figure 3; however, the complexity of the patterns was far greater since there were more open channels available at higher incident energy ($\mathscr{N}_{1,+} = \mathscr{N}_{1,-} = \{0, \pm1, \pm2, \pm3\}$ and $\mathscr{N}_{2,+} = \mathscr{N}_{2,-} = \{0, \pm1, \pm2\}$ in figure 4(B)).

4. Conclusion

In this work, a theory for the two-dimensional scattering of plane-waves from a periodic, quasi-one-dimensional potential comprised of nonmagnetic, localized scatterers in the presence of Rashba spin–orbit coupling was presented. Formulas for both the transmitted and reflected wave functions along with the spin subband resolved transmission and reflection coefficients were derived along with conditions for the occurrence of *interspin* and/or *intraspin* subband interference in the transmitted probability density. Finally, the effects of spin–orbit coupling on the Talbot effect were investigated. It was demonstrated that for an incident wave in either the '±'-spin subband, different Talbot lengths due to both *intraspin* and *interspin* subband interference can be found in the transmitted wave function. Numerical simulations were

presented that support many of the theoretical conclusions presented in this work. Besides providing a theoretical solution to a very fundamental textbook problem of two-dimensional scattering from a diffraction grating in the presence of spin–orbit coupling, the results from this work should be useful to experimentalists studying coherent transport in effective two-dimensional systems such as in 2DEGs, and in optical studies of ultracold atomic [30] and photonic lattices [31] and in band-engineered photonic crystals [32].

Acknowledgments

This work was supported by the National Science Foundation under CHE—1807724 and a Provost Research Award from the University of Miami. The numerical simulations presented in this work were conducted in part using resources of the University of Miami Center for Computational Science. Matlab programs that were used in this work are available upon request.

Appendix A. Multiple Scattering Theory for a quasi-one-dimensional scattering array

In this section, the details of the calculations leading to the transmitted and reflected wave functions, $\Psi^{\pm}_{\mathscr{T}}(\vec{r})$ in equation (10) and $\Psi^{\pm}_{\mathscr{R}}(\vec{r})$ in equation (12), are presented. The theory follows a similar treatment that was presented for the case of multiple scattering in single-layer graphene [16]. For an incident plane-wave in the $\pm$-spin subband, $\phi^{\pm}_{\vec{k}_{\pm}}(\vec{r})$ (equation (3)), that scatters from a quasi-one-dimensional scattering array $V(\vec{r})$ given in equation (4), Bloch's theorem states that $\Psi^{\pm}(\vec{r})$ can be written as:

$$\Psi^{\pm}(\vec{r}) = \phi^{\pm}_{\vec{k}_{\pm}}(\vec{r}) + \sum_{m=1}^{N_c}\sum_{l=-\infty}^{\infty} \widehat{G}^{(m)}_{0,l}(\vec{r}-\vec{r}_m, d, k_{Y,\pm}, E)\widehat{T}_l\Psi^{\pm}(\vec{r}_m), \tag{A.1}$$

where $\widehat{T}_l = \begin{pmatrix} \widehat{P}_l & 0 \\ 0 & \widehat{P}_{-l} \end{pmatrix}$ with $\widehat{P}_0 = \hat{1}$ and $\widehat{P}_l = \frac{1}{\bar{k}^{|l|}}\left(-\mathrm{i}\frac{\partial}{\partial x} + \frac{l}{|l|}\frac{\partial}{\partial y}\right)^{|l|} = \left(-\frac{\mathrm{i}}{\bar{k}}\right)^{|l|}\left(\mathrm{e}^{\pm\mathrm{i}\theta}\left(\frac{\partial}{\partial r} \pm \frac{\mathrm{i}}{r}\frac{\partial}{\partial\theta}\right)\right)^{|l|}$ for $l \neq 0$. For $|\Delta\vec{r}| \neq 0$:

$$\widehat{G}^{(m)}_{l',l}(\Delta\vec{r}, d, k_{Y,\pm}, E) = \frac{t_{1;l,a_m}}{2}\left(\frac{k_1}{\bar{k}}\right)^{|l'|}\begin{pmatrix} SS_{l'-l}(k_1, k_{Y,\pm}, d, \Delta\vec{r}) & \mathrm{i}SS_{l+l'-1}(k_1, k_{Y,\pm}, d, \Delta\vec{r}) \\ -\mathrm{i}SS_{-(l+l'-1)}(k_1, k_{Y,\pm}, d, \Delta\vec{r}) & SS_{l-l'}(k_1, k_{Y,\pm}, d, \Delta\vec{r}) \end{pmatrix} + \frac{t_{2;l,a_m}}{2}\left(\frac{k_2}{\bar{k}}\right)^{|l'|}\begin{pmatrix} SS_{l'-l}(k_2, k_{Y,\pm}, d, \Delta\vec{r}) & -\mathrm{i}SS_{l+l'-1}(k_2, k_{Y,\pm}, d, \Delta\vec{r}) \\ \mathrm{i}SS_{-(l+l'-1)}(k_2, k_{Y,\pm}, d, \Delta\vec{r}) & SS_{l-l'}(k_2, k_{Y,\pm}, d, \Delta\vec{r}) \end{pmatrix}, \tag{A.2}$$

where $t_{1;l,a_m}$ and $t_{2;l,a_m}$ are the scattering coefficients for the mth scatterer (explicit formula for $t_{1;l,a_m}$ and $t_{2;l,a_m}$ are given in appendix B for the case when the scatterers are represented by a step potential in equation (4)) and where:

$$SS_l(k_b, k_{Y,\pm}, d, \Delta\vec{r}) = \mathrm{i}^l\sum_{n=-\infty}^{\infty} H_l^+(k_b|\Delta\vec{r}^{(n)}|)\mathrm{e}^{\mathrm{i}l\theta_{\Delta\vec{r}^{(n)}}}\mathrm{e}^{\mathrm{i}nk_{Y,\pm}d} \tag{A.3}$$

with $H_l^+(x) = J_l(x) + \mathrm{i}Y_l(x)$ being a Hankel function of the first kind, $\Delta\vec{r}^{(n)} = \Delta\vec{r} - nd\hat{y}$, and $\mathrm{e}^{\mathrm{i}l\theta_{\Delta\vec{r}^{(n)}}} = \left(\frac{\Delta\vec{r}^{(n)}\cdot(\hat{x}+\mathrm{i}\hat{y})}{|\Delta\vec{r}^{(n)}|}\right)^l$. There are in general two ways to evaluate $SS_l(k_b, k_{Y,\pm}, d, \Delta\vec{r})$ in equation (A.3) depending upon the size of $|\hat{x}\cdot\Delta\vec{r}|$. When $|\hat{x}\cdot\Delta\vec{r}| \geqslant \frac{d}{2}$, $SS_l(k_b, k_{Y,\pm}, d, \Delta\vec{r})$ can be efficiently calculated using a plane-wave expansion [33]:

$$\begin{aligned} SS_l(k_b, k_{Y,\pm}, d, \Delta\vec{r}) &= \mathrm{i}^l\sum_{n=-\infty}^{\infty} H_l^+(k_b|\Delta\vec{r}^{(n)}|)\mathrm{e}^{\mathrm{i}l\theta_{\Delta\vec{r}^{(n)}}}\mathrm{e}^{\mathrm{i}nk_{Y,\pm}d} \\ &= \frac{(-\mathrm{i})^{|l|}}{k_b^{|l|}}\left(\frac{\partial}{\partial x} + \mathrm{i}\frac{l}{|l|}\frac{\partial}{\partial y}\right)^{|l|}\left[\sum_{n=-\infty}^{\infty} H_0^+(k_b|\Delta\vec{r}^{(n)}|)\mathrm{e}^{\mathrm{i}nk_{Y,\pm}d}\right] \\ &= \frac{2}{d}\sum_{n=-\infty}^{\infty}\frac{\mathrm{e}^{\mathrm{i}(k^{(n)}_{Y,\pm}\hat{y}\cdot\Delta\vec{r} + k^{(n)}_{bX,\pm}|\hat{x}\cdot\Delta\vec{r}|)}}{k^{(n)}_{bX,\pm}}([\mathrm{sign}(\hat{x}\cdot\Delta\vec{r})]^l\mathrm{e}^{\mathrm{i}l[\mathrm{sign}(\hat{x}\cdot\Delta\vec{r})\theta_{\vec{k}^{(n)}_{b,\pm}}]}), \end{aligned} \tag{A.4}$$

where $k_b = k_1$ or $k_b = k_2$, and where $\vec{k}^{(n)}_{b\pm} = k^{(n)}_{bX,\pm}\hat{x} + k^{(n)}_{Y,\pm}\hat{y}$ with $k^{(n)}_{Y,\pm} = k_{Y,\pm} + \frac{2\pi n}{d}$. For $k_b \geqslant k^{(n)}_{Y,\pm}$, $k^{(n)}_{bX,\pm} = \sqrt{k_b^2 - (k^{(n)}_{Y,\pm})^2}$ and $\mathrm{e}^{\mathrm{i}\theta_{\vec{k}^{(n)}_{b,\pm}}} = \frac{\vec{k}^{(n)}_{b,\pm}\cdot(\hat{x}+\mathrm{i}\hat{y})}{k_b}$. For $k_b \leqslant k^{(n)}_{Y,\pm}$, $k^{(n)}_{bX,\pm} = \mathrm{i}\sqrt{(k^{(n)}_{Y,\pm})^2 - k_b^2}$ with $\mathrm{e}^{\mathrm{i}\theta_{\vec{k}^{(n)}_{b,\pm}}} = \mathrm{i}\frac{|k^{(n)}_{bX,\pm}| + k^{(n)}_{Y,\pm}}{k_b}$ and $\mathrm{e}^{-\mathrm{i}\theta_{\vec{k}^{(n)}_{b,\pm}}} = \mathrm{i}\frac{|k^{(n)}_{bX,\pm}| - k^{(n)}_{Y,\pm}}{k_b}$. Note that $k^{(n)}_{bX,\pm}$ will be real for integers $n \in \mathscr{N}_{b,\pm}$ in equation (6).

The requirement that $|\hat{x}\cdot\Delta\vec{r}| \geqslant \frac{d}{2}$ insures that the summation in equation (A.4) can be approximated using only a finite number of evanescent waves. For $|\hat{x}\cdot\Delta\vec{r}| \leqslant \frac{d}{2}$, on the other hand, the convergence of equation (A.4) is slow due to the necessity of including a large number of evanescent waves in the calculation. In this case, $SS_l(k_b, k_{Y,\pm}, d, \Delta\vec{r})$ in equation (A.3) can be calculated using Graf's theorem [33, 34] as:

$$\begin{aligned} SS_l(k_b, k_{Y,\pm}, d, \Delta\vec{r}) &= \mathrm{i}^l H_l^+(k_b|\Delta\vec{r}|)\mathrm{e}^{\mathrm{i}l\theta_{\Delta\vec{r}}} \\ &+ \sum_{n=-\infty}^{\infty} S_{|n|}(k_b, k_{Y,\pm}, d)\mathrm{i}^{l-|n|}J_{n+l}(k_b|\Delta\vec{r}|)\mathrm{e}^{\mathrm{i}(n+l)\theta_{\Delta\vec{r}}}, \end{aligned} \tag{A.5}$$

where the lattice sums, $S_l(k_b, k_{Y,\pm}, d)$ can be efficiently calculated using [34, 35]:

$$S_l(k_b, k_{Y,\pm}, d) = \sum_{n=1}^{\infty} H_l^+(nk_b d)(\mathrm{e}^{\mathrm{i}nk_{Y,\pm}d} + (-1)^l \mathrm{e}^{-\mathrm{i}nk_{Y,\pm}d})$$
$$= \frac{\sqrt{2}}{\pi}\mathrm{e}^{-\mathrm{i}\left(\frac{\pi}{4}-k_{Y,\pm}d\right)} \int_0^{b_{\lim}} \mathrm{d}t \frac{[(t(1-\mathrm{i}) - \mathrm{i}\sqrt{1+2\mathrm{i}t^2})^l + (t(\mathrm{i}-1) - \mathrm{i}\sqrt{1+2\mathrm{i}t^2})^l]\mathrm{e}^{\mathrm{i}k_b d\sqrt{1+2\mathrm{i}t^2}}}{\sqrt{1+2\mathrm{i}t^2}(1-\mathrm{e}^{\mathrm{i}(k_b d\sqrt{1+2\mathrm{i}t^2}+k_{Y,\pm}d)})}$$
$$+ (-1)^l \frac{\sqrt{2}}{\pi}\mathrm{e}^{-\mathrm{i}\left(\frac{\pi}{4}+k_{Y,\pm}d\right)} \int_0^{b_{\lim}} \mathrm{d}t \frac{[(t(1-\mathrm{i}) - \mathrm{i}\sqrt{1+2\mathrm{i}t^2})^l + (t(\mathrm{i}-1) - \mathrm{i}\sqrt{1+2\mathrm{i}t^2})^l]\mathrm{e}^{\mathrm{i}k_b d\sqrt{1+2\mathrm{i}t^2}}}{\sqrt{1+2\mathrm{i}t^2}(1-\mathrm{e}^{\mathrm{i}(k_b d\sqrt{1+2\mathrm{i}t^2}-k_{Y,\pm}d)})}. \quad (A.6)$$

In this work, equation (A.6) was numerically integrated using MATLAB [36] with $b_{\lim} = 4000$.

For $|\Delta\vec{r}| = 0$, $\widehat{G}^{(m)}_{l',l}(\Delta\vec{r}, d, k_{Y,\pm}, E)$ is replaced by $\widetilde{G}^{D,(m)}_{l',l}(d, k_{Y,\pm}, E)$, which is given by:

$$\widetilde{G}^{D,(m)}_{l',l}(d, k_{Y,\pm}, E)$$
$$= \lim_{\Delta\vec{r}\to 0}(\widehat{G}^{(m)}_{l',l}(\Delta\vec{r}, d, k_{Y,\pm}, E) - \widehat{G}^{R,(m)}_{l',l}(\Delta\vec{r}, d, k_{Y,\pm}, E))$$
$$= \frac{t_{1;l,a_m}}{2}\left(\frac{k_1}{\bar{k}}\right)^{|l'|}\begin{pmatrix} S_{l'-l}(k_1, k_{Y,\pm}, d) & \mathrm{i}S_{l'+l-1}(k_1, k_{Y,\pm}, d) \\ -\mathrm{i}S_{-(l'+l-1)}(k_1, k_{Y,\pm}, d) & S_{l-l'}(k_1, k_{Y,\pm}, d)\end{pmatrix}$$
$$+ \frac{t_{2;l,a_m}}{2}\left(\frac{k_2}{\bar{k}}\right)^{|l'|}\begin{pmatrix} S_{l'-l}(k_2, k_{Y,\pm}, d) & -\mathrm{i}S_{l'+l-1}(k_2, k_{Y,\pm}, d) \\ \mathrm{i}S_{-(l'+l-1)}(k_2, k_{Y,\pm}, d) & S_{l-l'}(k_2, k_{Y,\pm}, d)\end{pmatrix}, \quad (A.7)$$

where $\widehat{G}^{R,(m)}_{l',l}(\vec{r}, d, k_{Y,\pm}, E)$ was used to remove the singularity in $\widehat{G}^{(m)}_{l',l}(\Delta\vec{r}, d, k_{Y,\pm}, E)$ as $|\Delta\vec{r}| \to 0$ and is given by:

$$\widehat{G}^{R,(m)}_{l',l}(\vec{r}, d, k_{Y,\pm}, E) = \frac{t_{1;l,a_m}}{2}\left(\frac{k_1}{\bar{k}}\right)^{|l'|}\begin{pmatrix} \mathrm{i}^{l'-l}H^+_{l'-l}(k_1|\vec{r}|)\mathrm{e}^{\mathrm{i}(l'-l)\theta_{\Delta\vec{r}^{(0)}}} & \mathrm{i}^{l'+l}H^+_{l'+l-1}(k_1|\vec{r}|)\mathrm{e}^{\mathrm{i}(l'+l-1)\theta_{\vec{r}}} \\ -\mathrm{i}^{l+l'}H^+_{l+l'-1}(k_1|\vec{r}|)\mathrm{e}^{-\mathrm{i}(l+l'-1)\theta_{\vec{r}}} & \mathrm{i}^{l-l'}H_{l-l'}(k_1|\vec{r}|)\mathrm{e}^{\mathrm{i}(l-l')\theta_{\vec{r}}}\end{pmatrix}$$
$$+ \frac{t_{2;l,a_m}}{2}\left(\frac{k_2}{\bar{k}}\right)^{|l'|}\begin{pmatrix} \mathrm{i}^{l'-l}H^+_{l'-l}(k_2|\vec{r}|)\mathrm{e}^{\mathrm{i}(l'-l)\theta_{\Delta\vec{r}^{(0)}}} & -\mathrm{i}^{l'+l}H^+_{l'+l-1}(k_2|\vec{r}|)\mathrm{e}^{\mathrm{i}(l'+l-1)\theta_{\vec{r}}} \\ \mathrm{i}^{l+l'}H^+_{l+l'-1}(k_2|\vec{r}|)\mathrm{e}^{-\mathrm{i}(l+l'-1)\theta_{\vec{r}}} & \mathrm{i}^{l-l'}H_{l-l'}(k_2|\vec{r}|)\mathrm{e}^{\mathrm{i}(l-l')\theta_{\vec{r}}}\end{pmatrix}. \quad (A.8)$$

While in principle an infinite number of scattering harmonics need to be included in the exact calculation of $\Psi^{\pm}(\vec{r})$ in equation (A.1), $\Psi^{\pm}(\vec{r})$ can generally be safely approximated by using only $2l_{\max}+1$ scattering harmonics as:

$$\Psi^{\pm}(\vec{r}) \approx \phi^{\pm}_{\vec{k}_{\pm}}(\vec{r}) + \sum_{m=1}^{N_s}\sum_{l=-l_{\max}}^{l_{\max}} \widehat{G}^{(m)}_{0,l}(\vec{r}-\vec{r}_m, d, k_{Y,\pm}, E)\widehat{T}_l\Psi^{\pm}(\vec{r}_m). \quad (A.9)$$

As such, knowledge of $\widehat{T}_l\Psi^{\pm}(\vec{r}_m)$ for $m = 1$ to $m = N_s$ and for $l \in [-l_{\max},\cdots,l_{\max}]$ completely determines $\Psi^{\pm}(\vec{r})$ in equation (A.9). The various values for $\widehat{T}_l\Psi^{\pm}(\vec{r}_m)$ can be determined self-consistently using the Foldy–Lax method [37, 38]:

$$\widehat{T}_{l'}\Psi^{\pm}(\vec{r}_m) = \widehat{T}_{l'}\phi^{\pm}_{\vec{k}_{\pm}}(\vec{r}_m) + \sum_{l=-l_{\max}}^{l_{\max}} \widehat{G}^{D,(m)}_{l',l}(d, k_{Y,\pm}, E)\widehat{T}_l\Psi^{\pm}(\vec{r}_m)$$
$$+ \sum_{p\neq m}^{N_s}\sum_{l=-l_{\max}}^{l_{\max}} \widehat{G}^{(p)}_{l',l}(\Delta\vec{r}_{m,p}, d, k_{Y,\pm}, E)\widehat{T}_l\Psi^{\pm}(\vec{r}_p) \quad (A.10)$$

for $l' \in [-l_{\max},\ldots,l_{\max}]$, $m \in [1,\ldots,N_s]$ and with $\Delta\vec{r}_{m,p} = \vec{r}_m - \vec{r}_p$. In writing equation (A.10), the relationships $\widehat{T}_{l'}\widehat{G}^{(m)}_{a,b}(\Delta\vec{r}, d, k_{Y,\pm}, E) = \widehat{G}^{(m)}_{a+l',b}(\Delta\vec{r}, d, k_{Y,\pm}, E)$ and $\widehat{T}_{l'}\widehat{G}^{D,(m)}_{a,b}(d, k_{Y,\pm}, E) = \widehat{G}^{D,(m)}_{a+l',b}(d, k_{Y,\pm}, E)$ were used.

Equation (A.10) represents a set of $2N_s(2l_{\max}+1)$ equations that can be written compactly as:

$$(\hat{\hat{\mathbf{1}}} - \widehat{\widehat{\mathbf{TG}}}(d, k_{Y,\pm}, E))\widehat{\widehat{\mathbf{T}}}\widehat{\Psi}^{\pm}(\vec{R}_0) = \widehat{\widehat{\mathbf{T}}}\widehat{\phi}^{\pm}_{\vec{k}_{\pm}}(\vec{R}_0), \quad (A.11)$$

where $\vec{R}_0 = \{\vec{r}_1, \vec{r}_2,\ldots,\vec{r}_{N_s}\}$ is a vector of all N_s scatterer positions in the $n = 0$ unit cell, $\hat{\hat{\mathbf{1}}}$ is the $2N_s(2l_{\max}+1) \times 2N_s(2l_{\max}+1)$ identity matrix, $\widehat{\widehat{\mathbf{T}}}\widehat{\Psi}^{\pm}(\vec{R}_0)$ and $\widehat{\widehat{\mathbf{T}}}\widehat{\phi}^{\pm}_{\vec{k}_{\pm}}(\vec{R}_0)$ are $2N_s(2l_{\max}+1) \times 1$ column vectors given by:

$$\widehat{\widehat{\mathbf{T}}}\widehat{\Psi}^{\pm}(\vec{R}_0) = \begin{pmatrix} \widehat{\widehat{\mathbf{T}}}\widehat{\Psi}^{\pm}(\vec{r}_1) \\ \widehat{\widehat{\mathbf{T}}}\widehat{\Psi}^{\pm}(\vec{r}_2) \\ \widehat{\widehat{\mathbf{T}}}\widehat{\Psi}^{\pm}(\vec{r}_3) \\ \vdots \\ \widehat{\widehat{\mathbf{T}}}\widehat{\Psi}^{\pm}(\vec{r}_{N_s})\end{pmatrix}, \widehat{\widehat{\mathbf{T}}}\widehat{\phi}^{\pm}_{\vec{k}_{\pm}}(\vec{R}_0) = \begin{pmatrix} \widehat{\widehat{\mathbf{T}}}\widehat{\phi}^{\pm}_{\vec{k}_{\pm}}(\vec{r}_1) \\ \widehat{\widehat{\mathbf{T}}}\widehat{\phi}^{\pm}_{\vec{k}_{\pm}}(\vec{r}_2) \\ \widehat{\widehat{\mathbf{T}}}\widehat{\phi}^{\pm}_{\vec{k}_{\pm}}(\vec{r}_3) \\ \vdots \\ \widehat{\widehat{\mathbf{T}}}\widehat{\phi}^{\pm}_{\vec{k}_{\pm}}(\vec{r}_{N_s})\end{pmatrix} \quad (A.12)$$

with:

$$\widehat{\widehat{\mathbf{T}}}\widehat{\Psi}^{\pm}(\vec{r}_m) = \begin{pmatrix} \widehat{T}_{l_{\max}}\Psi^{\pm}(\vec{r}_m) \\ \widehat{T}_{l_{\max}-1}\Psi^{\pm}(\vec{r}_m) \\ \vdots \\ \Psi^{\pm}(\vec{r}_m) \\ \vdots \\ \widehat{T}_{-(l_{\max}-1)}\Psi^{\pm}(\vec{r}_m) \\ \widehat{T}_{-l_{\max}}\Psi^{\pm}(\vec{r}_m) \end{pmatrix}, \quad \widehat{\widehat{\mathbf{T}}}\widehat{\phi}_{\vec{k}_\pm}^{\pm}(\vec{r}_m) = \sqrt{\frac{m^* k_\pm}{2\hbar\bar{k}|\vec{k}_\pm \cdot \hat{n}|}}\, \mathrm{e}^{\mathrm{i}\vec{k}_\pm\cdot\vec{r}_m} \begin{pmatrix} \left(\frac{k_\pm}{\bar{k}}\right)^{|l_{\max}|}\mathrm{e}^{\mathrm{i}l_{\max}\theta_0} \\ \mp\mathrm{i}\left(\frac{k_\pm}{\bar{k}}\right)^{|l_{\max}|}\mathrm{e}^{-\mathrm{i}(l_{\max}-1)\theta_0} \\ \left(\frac{k_\pm}{\bar{k}}\right)^{|l_{\max}-1|}\mathrm{e}^{\mathrm{i}(l_{\max}-1)\theta_0} \\ \mp\mathrm{i}\left(\frac{k_\pm}{\bar{k}}\right)^{|l_{\max}-1|}\mathrm{e}^{-\mathrm{i}(l_{\max}-2)\theta_0} \\ \vdots \\ 1 \\ \mp\mathrm{i}\mathrm{e}^{\mathrm{i}\theta_0} \\ \vdots \\ \left(\frac{k_\pm}{\bar{k}}\right)^{|l_{\max}-1|}\mathrm{e}^{-\mathrm{i}(l_{\max}-1)\theta_0} \\ \mp\mathrm{i}\left(\frac{k_\pm}{\bar{k}}\right)^{|l_{\max}-1|}\mathrm{e}^{\mathrm{i}l_{\max}\theta_0} \\ \left(\frac{k_\pm}{\bar{k}}\right)^{|l_{\max}|}\mathrm{e}^{-\mathrm{i}l_{\max}\theta_0} \\ \mp\mathrm{i}\left(\frac{k_\pm}{\bar{k}}\right)^{|l_{\max}|}\mathrm{e}^{\mathrm{i}(l_{\max}+1)\theta_0} \end{pmatrix}. \tag{A.13}$$

In equation (A.11), $\widehat{\widehat{\mathbf{TG}}}(d, k_{Y,\pm}, E)$ is a $2N_s(2l_{\max}+1) \times 2N_s(2l_{\max}+1)$ matrix given by:

$$\widehat{\widehat{\mathbf{TG}}}(d, k_{Y,\pm}, E) = \begin{pmatrix} \widehat{\widehat{\mathbf{TG}}}_{(1,1)}(d, k_{Y,\pm}, E) & \widehat{\widehat{\mathbf{TG}}}_{(1,2)}(d, k_{Y,\pm}, E) & \dots & \widehat{\widehat{\mathbf{TG}}}_{(1,N_s)}(d, k_{Y,\pm}, E) \\ \widehat{\widehat{\mathbf{TG}}}_{(2,1)}(d, k_{Y,\pm}, E) & \widehat{\widehat{\mathbf{TG}}}_{(2,2)}(d, k_{Y,\pm}, E) & \dots & \widehat{\widehat{\mathbf{TG}}}_{(2,N_s)}(d, k_{Y,\pm}, E) \\ \vdots & \vdots & \ddots & \vdots \\ \widehat{\widehat{\mathbf{TG}}}_{(N_s,1)}(d, k_{Y,\pm}, E) & \widehat{\widehat{\mathbf{TG}}}_{(N_s,2)}(d, k_{Y,\pm}, E) & \dots & \widehat{\widehat{\mathbf{TG}}}_{(N_s,N_s)}(d, k_{Y,\pm}, E) \end{pmatrix}, \tag{A.14}$$

where

$$\widehat{\widehat{\mathbf{TG}}}_{(m,m)}(d, k_{Y,\pm}, E) = \begin{pmatrix} \widehat{G}^{D,(m)}_{l_{\max},l_{\max}}(d, k_{Y,\pm}, E) & \widehat{G}^{D,(m)}_{l_{\max},l_{\max}-1}(d, k_{Y,\pm}, E) & \dots & \widehat{G}^{D,(m)}_{l_{\max},-l_{\max}}(d, k_{Y,\pm}, E) \\ \widehat{G}^{D,(m)}_{l_{\max}-1,l_{\max}}(d, k_{Y,\pm}, E) & \widehat{G}^{D,(m)}_{l_{\max}-1,l_{\max}-1}(d, k_{Y,\pm}, E) & \dots & \widehat{G}^{D,(m)}_{l_{\max}-1,-l_{\max}}(d, k_{Y,\pm}, E) \\ \vdots & \vdots & \ddots & \vdots \\ \widehat{G}^{D,(m)}_{-l_{\max},l_{\max}}(d, k_{Y,\pm}, E) & \widehat{G}^{D,(m)}_{-l_{\max},l_{\max}-1}(d, k_{Y,\pm}, E) & \dots & \widehat{G}^{D,(m)}_{-l_{\max},-l_{\max}}(d, k_{Y,\pm}, E) \end{pmatrix} \tag{A.15}$$

and (for $m \neq n$):

$$\widehat{\widehat{\mathbf{TG}}}_{(m,n)}(d, k_{Y,\pm}, E) = \begin{pmatrix} \widehat{G}^{(n)}_{l_{\max},l_{\max}}(\Delta\vec{r}_{m,n}, d, k_{Y,\pm}, E)\,\widehat{G}^{(n)}_{l_{\max},l_{\max}-1}(\Delta\vec{r}_{m,n}, d, k_{Y,\pm}, E) & \dots & \widehat{G}^{(n)}_{l_{\max},-l_{\max}}(\Delta\vec{r}_{m,n}, d, k_{Y,\pm}, E) \\ \tilde{G}^{(n)}_{l_{\max}-1,l_{\max}}(\Delta\vec{r}_{m,n}, d, k_{Y,\pm}, E)\widehat{G}^{(n)}_{l_{\max}-1,l_{\max}-1}(\Delta\vec{r}_{m,n}, d, k_{Y,\pm}, E) & \dots & \widehat{G}^{(n)}_{l_{\max}-1,-l_{\max}}(\Delta\vec{r}_{m,n}, d, k_{Y,\pm}, E) \\ \vdots & \ddots & \vdots \\ \widehat{G}^{(n)}_{-l_{\max},l_{\max}}(\Delta\vec{r}_{m,n}, d, k_{Y,\pm}, E)\widehat{G}^{(n)}_{-l_{\max},l_{\max}-1}(\Delta\vec{r}_{m,n}, d, k_{Y,\pm}, E) & \dots & \widehat{G}^{(n)}_{-l_{\max},-l_{\max}}(\Delta\vec{r}_{m,n}, d, k_{Y,\pm}, E) \end{pmatrix}. \tag{A.16}$$

For $|x| \gg d$, $\Psi^{\pm}(\vec{r})$ in equation (A.9) can be written as a summation over plane and evanescent waves:

$$\Psi^{\pm}(\vec{r}) = \phi^{\pm}_{\vec{k}_{\pm}}(\vec{r}) + \sum_{m=1}^{N_s}\sum_{l=-l_{\max}}^{l_{\max}}\sum_{n\in\mathcal{N}_{1,\pm}} \frac{t_{1;l,\vec{r}_m} e^{ik^{(n)}_{Y,\pm}(\hat{y}\cdot(\vec{r}-\vec{r}_m))} e^{ik^{(n)}_{1X,\pm}|\hat{x}\cdot(\vec{r}-\vec{r}_m)|}}{k^{(n)}_{1X,\pm} d}[\mathrm{sign}(\hat{x}\cdot(\vec{r}-\vec{r}_m))]^l$$
$$\times\begin{pmatrix} e^{-il[\mathrm{sign}(\hat{x}\cdot(\vec{r}-\vec{r}_m))\theta_{\vec{k}^{(n)}_{1,\pm}}]} & i[\mathrm{sign}(\hat{x}\cdot(\vec{r}-\vec{r}_m))] e^{i(l-1)[\mathrm{sign}(\hat{x}\cdot(\vec{r}-\vec{r}_m))\theta_{\vec{k}^{(n)}_{1,\pm}}]} \\ -i[\mathrm{sign}(\hat{x}\cdot(\vec{r}-\vec{r}_m))] e^{-i(l-1)[\mathrm{sign}(\hat{x}\cdot(\vec{r}-\vec{r}_m))\theta_{\vec{k}^{(n)}_{1,\pm}}]} & e^{il[\mathrm{sign}(\hat{x}\cdot(\vec{r}-\vec{r}_m))\theta_{\vec{k}^{(n)}_{1,\pm}}]} \end{pmatrix}\widehat{T}_l\Psi^{\pm}(\vec{r}_m)$$
$$+\sum_{m=1}^{N_s}\sum_{l=-l_{\max}}^{l_{\max}}\sum_{n\in\mathcal{N}_{2,\pm}} \frac{t_{2;l,\vec{r}_m} e^{ik^{(n)}_{Y,\pm}(\hat{y}\cdot(\vec{r}-\vec{r}_m))} e^{ik^{(n)}_{2X,\pm}|\hat{x}\cdot(\vec{r}-\vec{r}_m)|}}{k^{(n)}_{2X,\pm} d}[\mathrm{sign}(\hat{x}\cdot(\vec{r}-\vec{r}_m))]^l$$
$$\times\begin{pmatrix} e^{-il[\mathrm{sign}(\hat{x}\cdot(\vec{r}-\vec{r}_m))\theta_{\vec{k}^{(n)}_{2,\pm}}]} & -i[\mathrm{sign}(\hat{x}\cdot(\vec{r}-\vec{r}_m))] e^{i(l-1)[\mathrm{sign}(\hat{x}\cdot(\vec{r}-\vec{r}_m))\theta_{\vec{k}^{(n)}_{2,\pm}}]} \\ i[\mathrm{sign}(\hat{x}\cdot(\vec{r}-\vec{r}_m))] e^{-i(l-1)[\mathrm{sign}(\hat{x}\cdot(\vec{r}-\vec{r}_m))\theta_{\vec{k}^{(n)}_{2,\pm}}]} & e^{il[\mathrm{sign}(\hat{x}\cdot(\vec{r}-\vec{r}_m))\theta_{\vec{k}^{(n)}_{2,\pm}}]} \end{pmatrix}\widehat{T}_l\Psi^{\pm}(\vec{r}_m)$$
$$-\sum_{m=1}^{N_s}\sum_{l=-l_{\max}}^{l_{\max}}\sum_{n\notin\mathcal{N}_{1,\pm}} \frac{it_{1;l,\vec{r}_m} e^{ik^{(n)}_{Y,\pm}(\hat{y}\cdot(\vec{r}-\vec{r}_m))} e^{-|k^{(n)}_{1X,\pm}||\hat{x}\cdot(\vec{r}-\vec{r}_m)|}}{k^{(n)}_{1X,\pm} d}[\mathrm{sign}(\hat{x}\cdot(\vec{r}-\vec{r}_m))]^l$$
$$\times\begin{pmatrix} e^{-il[\mathrm{sign}(\hat{x}\cdot(\vec{r}-\vec{r}_m))\theta_{\vec{k}^{(n)}_{1,\pm}}]} & i[\mathrm{sign}(\hat{x}\cdot(\vec{r}-\vec{r}_m))] e^{i(l-1)[\mathrm{sign}(\hat{x}\cdot(\vec{r}-\vec{r}_m))\theta_{\vec{k}^{(n)}_{1,\pm}}]} \\ -i[\mathrm{sign}(\hat{x}\cdot(\vec{r}-\vec{r}_m))] e^{-i(l-1)[\mathrm{sign}(\hat{x}\cdot(\vec{r}-\vec{r}_m))\theta_{\vec{k}^{(n)}_{1,\pm}}]} & e^{il[\mathrm{sign}(\hat{x}\cdot(\vec{r}-\vec{r}_m))\theta_{\vec{k}^{(n)}_{1,\pm}}]} \end{pmatrix}\widehat{T}_l\Psi^{\pm}(\vec{r}_m)$$
$$-\sum_{m=1}^{N_s}\sum_{l=-l_{\max}}^{l_{\max}}\sum_{n\notin\mathcal{N}_{2,\pm}} \frac{it_{2;l,\vec{r}_m} e^{ik^{(n)}_{Y,\pm}(\hat{y}\cdot(\vec{r}-\vec{r}_m))} e^{-|k^{(n)}_{2X,\pm}||\hat{x}\cdot(\vec{r}-\vec{r}_m)|}}{|k^{(n)}_{2X,\pm}|\, d}[\mathrm{sign}(\hat{x}\cdot(\vec{r}-\vec{r}_m))]^l$$
$$\times\begin{pmatrix} e^{-il[\mathrm{sign}(\hat{x}\cdot(\vec{r}-\vec{r}_m))\theta_{\vec{k}^{(n)}_{2,\pm}}]} & -i[\mathrm{sign}(\hat{x}\cdot(\vec{r}-\vec{r}_m))] e^{i(l-1)[\mathrm{sign}(\hat{x}\cdot(\vec{r}-\vec{r}_m))\theta_{\vec{k}^{(n)}_{2,\pm}}]} \\ i[\mathrm{sign}(\hat{x}\cdot(\vec{r}-\vec{r}_m))] e^{-i(l-1)[\mathrm{sign}(\hat{x}\cdot(\vec{r}-\vec{r}_m))\theta_{\vec{k}^{(n)}_{2,\pm}}]} & e^{il[\mathrm{sign}(\hat{x}\cdot(\vec{r}-\vec{r}_m))\theta_{\vec{k}^{(n)}_{2,\pm}}]} \end{pmatrix}\widehat{T}_l\Psi^{\pm}(\vec{r}_m) \quad \text{(A.17)}$$

In equation (A.17), the first two triple summations in $\Psi^{\pm}(\vec{r})$ consist of a series of plane-waves in the '+'-spin subband $[n \in \mathcal{N}_{1,\pm}]$ and in the '−'-spin subband $[n \in \mathcal{N}_{2,\pm}]$ that represent either transmitted $[x > 0]$ or reflected $[x < 0]$ waves, while the last two triple summations represent the contributions to $\Psi^{\pm}(\vec{r})$ from an infinite number of scattered evanescent waves for $n \notin \mathcal{N}_{1,\pm}$ and $m \notin \mathcal{N}_{2,\pm}$. For $|x| \gg d$, the contribution of these evanescent waves to $\Psi^{\pm}(\vec{r})$ becomes exponentially small leaving only the contributions from the 'open' channels that correspond to transmitted/reflected waves.

Appendix B. Scattering amplitudes for a cylindrically symmetric barrier/well

In this section, expressions for the scattering coefficients $t_{1;l,a_m}$ and $t_{2;l,a_m}$ for $E > 0$ are presented for a cylindrically symmetric potential well/barrier, $\widehat{V}(\vec{r}) = V\Theta_{a_m}(\vec{r})$ in equation (5), where a_m is the scatterer's radius. Both $t_{1;l,a_m}$ and $t_{2;l,a_m}$ were previously calculated [19] by enforcing the continuity of both the wave function and flux at the scatterer's boundary. For an incident plane-wave $\phi^{\pm}_{\vec{k}_{\pm}}(\vec{r})$ in equation (3) with $\vec{k}_{\pm} = k_{\pm}(\cos(\theta_0)\hat{x} + \sin(\theta_0)\hat{y})$, the overall wave function outside the scatterer (with the origin take to be at the scatterer's center) is given by:

$$\Psi^{\pm}(\vec{r}) = \phi^{\pm}_{\vec{k}_{\pm}}(\vec{r}) + \Psi^{\pm}_S(\vec{r}), \quad \text{(B.1)}$$

where $\Psi^{\pm}_S(\vec{r})$ is the scattered wave function given by:

$$\Psi^{\pm}_S(\vec{r}) = \sum_{l=-\infty}^{\infty}\lambda^{\pm}_l\left(\frac{\widetilde{f}^{\pm 1}_l}{\sqrt{k_1}}\chi_{l,1}(\vec{r}) + \frac{\widetilde{f}^{\pm 2}}{\sqrt{k_2}}\chi_{l,2}(\vec{r})\right), \quad \text{(B.2)}$$

where

$$\lambda^{\pm}_l = 2e^{il\theta_0}\sqrt{\frac{k_{\pm}}{\vec{k}_{\pm}\cdot\hat{n}}}$$
$$\chi_{l,1}(\vec{r}) = \frac{i^l}{2}\sqrt{\frac{m^* k_1}{2\hbar\bar{k}}}e^{-il\theta}\begin{pmatrix} H^+_l(k_1 r) \\ -H^+_{l-1}(k_1 r)e^{i\theta}\end{pmatrix}$$
$$\chi_{l,2}(\vec{r}) = \frac{i^l}{2}\sqrt{\frac{m^* k_2}{2\hbar\bar{k}}}e^{-il\theta}\begin{pmatrix} H^+_l(k_2 r) \\ H^+_{l-1}(k_2 r)e^{i\theta}\end{pmatrix}. \quad \text{(B.3)}$$

Defining the magnitudes of the wave vectors within the potential, κ_1 and κ_2 as:

$$\kappa_1 = k_\alpha + \sqrt{\left(\frac{m^*\alpha}{\hbar^2}\right)^2 + \frac{2m^*(E-V)}{\hbar^2}} = \frac{m^*\alpha}{\hbar^2} + \overline{\kappa}$$
$$\kappa_2 = -k_\alpha + \overline{\kappa} \quad \text{(B.4)}$$

one can solve for the coefficients $\widetilde{f}^{\pm 1}_l$ and $\widetilde{f}^{\pm 2}_l$ by enforcing continuity of both the wave function and the flux at the

scatterer's boundary at $|\vec{r}| = a_m$. Defining the functions

$$\begin{aligned}
JJ_l^{\pm}(k_a, k_b) &= J_l(k_a a_m)J_{l-1}(k_b a_m) \pm J_{l-1}(k_a a_m)J_l(k_b a_m)\\
HJ_l^{\pm}(k_a, k_b) &= H_l^{+}(k_a a_m)J_{l-1}(k_b a_m) \pm H_{l-1}^{+}(k_a a_m)J_l(k_b a_m)\\
\Delta JJJJ_l^{b,c}(z_a, z_b, k_c) &= z_a JJ_l^{b}(k_c, \kappa_2)JJ_l^{c}(\kappa_1, \kappa_2)\\
&\quad - z_b JJ_l^{-b}(k_c, \kappa_2)JJ_l^{-c}(\kappa_1, \kappa_2)\\
\Delta HJJJ_l^{b,c}(z_a, z_b, k_c) &= z_a HJ_l^{b}(k_c, \kappa_2)JJ_l^{c}(\kappa_1, \kappa_2)\\
&\quad - z_b HJ_l^{-b}(k_c, \kappa_2)JJ_l^{-c}(\kappa_1, \kappa_2)
\end{aligned} \tag{B.5}$$

the scattering coefficients can be written as:

$$\begin{aligned}
\widetilde{f}_l^{\pm 1} &= \frac{\Delta JJJJ_l^{\mp,+}\left(\frac{\kappa_2 \pm k_\pm}{\kappa_1+\kappa_2}, 1, k_\pm\right)\Delta HJJJ_l^{+,+}\left(\frac{\kappa_2-k_2}{\kappa_1+\kappa_2}, -\frac{k_2}{\kappa_1}, k_2\right) - \Delta JJJJ_l^{\mp,+}\left(\frac{\kappa_2 \pm k_\pm}{\kappa_1+\kappa_2}, \pm\frac{k_\pm}{\kappa_1}, k_\pm\right)\Delta HJJJ_l^{+,+}\left(\frac{\kappa_2-k_2}{\kappa_1+\kappa_2}, 1, k_2\right)}{\Delta HJJJ_l^{-,+}\left(\frac{k_1+\kappa_2}{\kappa_2+\kappa_1}, \frac{k_1}{\kappa_1}, k_1\right)\Delta HJJJ_l^{+,+}\left(\frac{\kappa_2-k_2}{\kappa_1+\kappa_2}, 1, k_2\right) - \Delta HJJJ_l^{-,+}\left(\frac{k_1+\kappa_2}{\kappa_2+\kappa_1}, 1, k_1\right)\Delta HJJJ_l^{+,+}\left(\frac{\kappa_2-k_2}{\kappa_1+\kappa_2}, -\frac{k_2}{\kappa_1}, k_2\right)}\\
\widetilde{f}_l^{\pm 2} &= \frac{\Delta JJJJ_l^{\mp,+}\left(\frac{\kappa_2 \pm k_\pm}{\kappa_1+\kappa_2}, 1, k_\pm\right)\Delta HJJJ_l^{-,+}\left(\frac{\kappa_2+k_1}{\kappa_1+\kappa_2}, \frac{k_1}{\kappa_1}, k_1\right) - \Delta JJJJ_l^{\mp,+}\left(\frac{\kappa_2 \pm k_\pm}{\kappa_1+\kappa_2}, \pm\frac{k_\pm}{\kappa_1}, k_\pm\right)\Delta HJJJ_l^{-,+}\left(\frac{\kappa_2+k_1}{\kappa_1+\kappa_2}, 1, k_1\right)}{\Delta HJJJ_l^{+,+}\left(\frac{\kappa_2-k_2}{\kappa_2+\kappa_1}, -\frac{k_2}{\kappa_1}, k_2\right)\Delta HJJJ_l^{-,+}\left(\frac{\kappa_2+k_1}{\kappa_1+\kappa_2}, 1, k_1\right) - \Delta HJJJ_l^{+,+}\left(\frac{\kappa_2-k_2}{\kappa_2+\kappa_1}, 1, k_2\right)\Delta HJJJ_l^{-,+}\left(\frac{\kappa_2+k_1}{\kappa_1+\kappa_2}, \frac{k_1}{\kappa_1}, k_1\right)},
\end{aligned} \tag{B.6}$$

where the various $\widetilde{f}_l^{\pm 1}$ and $\widetilde{f}_l^{\pm 2}$ satisfy the following unitarity conditions:

$$\begin{aligned}
-\text{Real}(\widetilde{f}_l^{+1}) &= |\widetilde{f}_l^{+1}|^2 + \frac{k_2}{k_1}|\widetilde{f}_l^{+2}|^2\\
-\text{Real}(\widetilde{f}_l^{-2}) &= |\widetilde{f}_l^{-2}|^2 + \frac{k_1}{k_2}|\widetilde{f}_l^{-1}|^2\\
\text{Real}(\widetilde{f}_l^{-2} - \widetilde{f}_l^{+1}) &= |\widetilde{f}_l^{+1}|^2 - |\widetilde{f}_l^{-2}|^2.
\end{aligned} \tag{B.7}$$

Finally, the individual scattering coefficients, $t_{1;l,a_m}$ and $t_{2;l,a_m}$ introduced in equation (A.2), can be related to $\widetilde{f}_l^{\pm 1}$ and $\widetilde{f}_l^{\pm 2}$ by:

$$\begin{aligned}
t_{1;l,a_m} &= 2\left(\frac{\bar{k}}{k_1 k_2}\right)^{|l|}\frac{k_2^{|l-1|}\widetilde{f}_l^{+1} + k_1^{|l-1|}\widetilde{f}_l^{-1}}{k_2^{|l-1|-|l|} + k_1^{|l-1|-|l|}}\\
t_{2;l,a_m} &= 2\left(\frac{\bar{k}}{k_1 k_2}\right)^{|l|}\frac{k_2^{|l-1|}\widetilde{f}_l^{+2} + k_1^{|l-1|}\widetilde{f}_l^{-2}}{k_2^{|l-1|-|l|} + k_1^{|l-1|-|l|}}\\
\widetilde{f}_l^{\pm 1} &= \frac{1}{2}\left(t_{1;l,a_m}\left(\frac{k_\pm}{\bar{k}}\right)^{|l|} \pm t_{1;-l+1,a_m}\left(\frac{k_\pm}{\bar{k}}\right)^{|l-1|}\right)\\
\widetilde{f}_l^{\pm 2} &= \frac{1}{2}\left(t_{2;l,a_m}\left(\frac{k_\pm}{\bar{k}}\right)^{|l|} \mp t_{2;-l+1,a_m}\left(\frac{k_\pm}{\bar{k}}\right)^{|l-1|}\right).
\end{aligned} \tag{B.8}$$

Appendix C. Local spin vector polarization density for the transmitted and reflected waves

The coefficients of the transmitted spin vector polarization density are given as:

$$\vec{P}^{\pm}_{\mathscr{T},\vec{\sigma}}(\vec{r}) = (P^{\pm}_{\mathscr{T},\hat{\sigma}_X}(\vec{r}), P^{\pm}_{\mathscr{T},\hat{\sigma}_Y}(\vec{r}), P^{\pm}_{\mathscr{T},\hat{\sigma}_Z}(\vec{r})) \tag{C.1}$$

with

$$\begin{aligned}
P^{\pm}_{\mathscr{T},\hat{\sigma}_Z}(\vec{r}) &= \sum_{a=1,2}\sum_{\substack{n,m\in\mathscr{N}_{a,\pm}\\ m<n}}\frac{k_a|\mathscr{T}^{(n)}_{a,\pm}\mathscr{T}^{(m)}_{a,\pm}|\sin(\phi^{(n,m)}_{a,a,\pm})}{\sqrt{k^{(n)}_{aX,\pm}k^{(m)}_{aX,\pm}}}\\
&\quad\times\sin((\vec{k}^{(n)}_{a,\pm} - \vec{k}^{(m)}_{a,\pm})\cdot\vec{r} + \Delta\theta_{\mathscr{T}^{(n,m)}_{a,a,\pm}})\\
&\quad + \sum_{n\in\mathscr{N}_{1,\pm}}\sum_{m\in\mathscr{N}_{2,\pm}}\frac{\sqrt{k_1k_2}|\mathscr{T}^{(n)}_{1,\pm}\mathscr{T}^{(m)}_{2,\pm}|\cos(\phi^{(n,m)}_{1,2,\pm})}{\sqrt{k^{(n)}_{1X,\pm}k^{(m)}_{2X,\pm}}}\\
&\quad\times\cos((\vec{k}^{(n)}_{1,\pm} - \vec{k}^{(m)}_{2,\pm})\cdot\vec{r} + \Delta\theta_{\mathscr{T}^{(n,m)}_{1,2,\pm}})
\end{aligned}, \tag{C.2}$$

$$\begin{aligned}
P^{\pm}_{\mathscr{T},\hat{\sigma}_X}(\vec{r}) &= -\sum_{a=1,2}\sum_{n\in\mathscr{N}_{a,\pm}}(-1)^a\frac{k_a|\mathscr{T}^{(n)}_{a,\pm}|^2}{2k^{(n)}_{aX,\pm}}\sin(\theta_{\vec{k}^{(n)}_{a,\pm}})\\
&\quad - \sum_{a=1,2}\sum_{\substack{n,m\in\mathscr{N}_{a,\pm}\\ m<n}}(-1)^a\frac{k_a|\mathscr{T}^{(n)}_{a,\pm}\mathscr{T}^{(m)}_{a,\pm}|\sin\left(\frac{\theta_{\vec{k}^{(n)}_{a,\pm}} + \theta_{\vec{k}^{(m)}_{a,\pm}}}{2}\right)}{\sqrt{k^{(n)}_{aX,\pm}k^{(m)}_{aX,\pm}}}\\
&\quad\times\cos((\vec{k}^{(n)}_{a,\pm} - \vec{k}^{(m)}_{a,\pm})\cdot\vec{r} + \Delta\theta_{\mathscr{T}^{(n,m)}_{a,a,\pm}})\\
&\quad + \sum_{n\in\mathscr{N}_{1,\pm}}\sum_{m\in\mathscr{N}_{2,\pm}}\frac{\sqrt{k_1k_2}|\mathscr{T}^{(n)}_{1,\pm}\mathscr{T}^{(m)}_{2,\pm}|\cos\left(\frac{\theta_{\vec{k}^{(n)}_{1,\pm}} + \theta_{\vec{k}^{(m)}_{2,\pm}}}{2}\right)}{\sqrt{k^{(n)}_{1X,\pm}k^{(m)}_{2X,\pm}}}\\
&\quad\times\sin((\vec{k}^{(n)}_{1,\pm} - \vec{k}^{(m)}_{2,\pm})\cdot\vec{r} + \Delta\theta_{\mathscr{T}^{(n,m)}_{1,2,\pm}})
\end{aligned} \tag{C.3}$$

and

$$\begin{aligned}
P^{\pm}_{\mathscr{T},\hat{\sigma}_Y}(\vec{r}) &= \sum_{a=1,2}\sum_{n\in\mathscr{N}_{a,\pm}}(-1)^a\frac{k_a|\mathscr{T}^{(n)}_{a,\pm}|^2}{2k^{(n)}_{aX,\pm}}\cos(\theta_{\vec{k}^{(n)}_{a,\pm}})\\
&\quad + \sum_{a=1,2}\sum_{\substack{n,m\in\mathscr{N}_{a,\pm}\\ m<n}}(-1)^a\frac{k_a|\mathscr{T}^{(n)}_{a,\pm}\mathscr{T}^{(m)}_{a,\pm}|\cos\left(\frac{\theta_{\vec{k}^{(n)}_{a,\pm}} + \theta_{\vec{k}^{(m)}_{a,\pm}}}{2}\right)}{\sqrt{k^{(n)}_{aX,\pm}k^{(m)}_{aX,\pm}}}\\
&\quad\times\cos((\vec{k}^{(n)}_{a,\pm} - \vec{k}^{(m)}_{a,\pm})\cdot\vec{r} + \Delta\theta_{\mathscr{T}^{(n,m)}_{a,a,\pm}})\\
&\quad + \sum_{n\in\mathscr{N}_{1,\pm}}\sum_{m\in\mathscr{N}_{2,\pm}}\frac{\sqrt{k_1k_2}|\mathscr{T}^{(n)}_{1,\pm}\mathscr{T}^{(m)}_{2,\pm}|\sin\left(\frac{\theta_{\vec{k}^{(n)}_{1,\pm}} + \theta_{\vec{k}^{(m)}_{2,\pm}}}{2}\right)}{\sqrt{k^{(n)}_{1X,\pm}k^{(m)}_{2X,\pm}}}\\
&\quad\times\sin((\vec{k}^{(n)}_{1,\pm} - \vec{k}^{(m)}_{2,\pm})\cdot\vec{r} + \Delta\theta_{\mathscr{T}^{(n,m)}_{1,2,\pm}}).
\end{aligned} \tag{C.4}$$

For the reflected wave, the dimensionless probability and spin vector polarization densities for $x \ll -d$ can be be calculated by:

$$\frac{\hbar\overline{k}}{m^*}\Psi^{\pm}_{\mathscr{R}}(\vec{r})(\Psi^{\pm}_{\mathscr{R}}(\vec{r}))^{\dagger} = \rho^{\pm}_{\mathscr{R}}(\vec{r})\,\hat{1} + \vec{P}^{\pm}_{\mathscr{R},\vec{\sigma}}(\vec{r})\cdot\vec{\boldsymbol{\sigma}}, \tag{C.5}$$

where $\rho^{\pm}_{\mathscr{R}}(\vec{r})$ and $\vec{P}^{\pm}_{\mathscr{R},\vec{\sigma}}(\vec{r}) = P^{\pm}_{\mathscr{R},\hat{\sigma}_X}(\vec{r})\hat{x} + P^{\pm}_{\mathscr{R},\hat{\sigma}_Y}(\vec{r})\hat{y} + P^{\pm}_{\mathscr{R},\hat{\sigma}_Z}(\vec{r})\hat{z}$ are the probability and spin vector polarization densities for the reflected wave function, respectively. Using equation (12) and writing the reflection coefficients as $\mathscr{R}^{(n)}_{1,\pm} = |\mathscr{R}^{(n)}_{1,\pm}|\exp\left(\mathrm{i}\left(\theta_{\mathscr{R}^{(n)}_{1,\pm}} + \frac{\theta_{\vec{k}^{(n)}_{1,\pm}}}{2}\right)\right)$ for $n \in \mathscr{N}_{1,\pm}$ and $\mathscr{R}^{(n)}_{2,\pm} = |\mathscr{R}^{(n)}_{2,\pm}|\exp\left(\mathrm{i}\left(\theta_{\mathscr{R}^{(n)}_{2,\pm}} + \frac{\theta_{\vec{k}^{(n)}_{2,\pm}}}{2}\right)\right)$ for $n \in \mathscr{N}_{2,\pm}$, $\rho^{\pm}_{\mathscr{R}}(\vec{r})$ can be written as:

$$\begin{aligned}
\rho^{\pm}_{\mathscr{R}}(\vec{r}) &= \frac{k_{\pm}}{2|\vec{k}_{\pm}\cdot\hat{x}|} + \sum_{a=1,2}\sum_{n\in\mathscr{N}_{a,\pm}}\frac{k_a\,|\mathscr{R}^{(n)}_{a,\pm}|^2}{2k^{(n)}_{aX,\pm}} \\
&+ \sum_{a=1,2}\sum_{\substack{n,m\in\mathscr{N}_{a,\pm}\\ m<n}}\frac{k_a|\mathscr{R}^{(n)}_{a,\pm}\mathscr{R}^{(m)}_{a,\pm}|\,\cos(\phi^{(n,m)}_{a,a,\pm})}{\sqrt{k^{(n)}_{aX,\pm}k^{(m)}_{aX,\pm}}} \\
&\times\cos((\overline{\vec{k}^{(n)}_{a,\pm}} - \overline{\vec{k}^{(m)}_{a,\pm}})\cdot\vec{r} + \Delta\theta_{\mathscr{R}^{(n,m)}_{a,a,\pm}}) \\
&- \sum_{n\in\mathscr{N}_{1,\pm}}\sum_{m\in\mathscr{N}_{2,\pm}}\frac{\sqrt{k_1k_2}\,|\mathscr{R}^{(n)}_{1,\pm}\mathscr{R}^{(m)}_{2,\pm}|\,\sin(\phi^{(n,m)}_{1,2,\pm})}{\sqrt{k^{(n)}_{1X,\pm}k^{(m)}_{2X,\pm}}} \\
&\times\sin((\overline{\vec{k}^{(n)}_{1,\pm}} - \overline{\vec{k}^{(m)}_{2,\pm}})\cdot\vec{r} + \Delta\theta_{\mathscr{R}^{(n,m)}_{1,2,\pm}}) \\
&+ \sum_{(a,b)\in\{(1,-),(2,+)\}}\sum_{n\in\mathscr{N}_{a,\pm}}\sqrt{\frac{k_1k_2}{k^{(n)}_{aX,\pm}|\vec{k}_b\cdot\hat{x}|}}\,\delta_{b,\pm}\cos\left(\frac{\theta_{\vec{k}^{(n)}_{a,\pm}}+\theta_0}{2}\right) \\
&\times\cos\left((\overline{\vec{k}^{(n)}_{a,\pm}} - \vec{k}_b)\cdot\vec{r} + \theta_{\mathscr{R}^{(n)}_{a,\pm}} - \frac{\theta_0}{2}\right) \\
&- \sum_{(a,b)\in\{(1,+),(2,-)\}}\sum_{n\in\mathscr{N}_{a,\pm}}\frac{k_a}{\sqrt{k^{(n)}_{aX,\pm}|\vec{k}_b\cdot\hat{x}|}}\,\delta_{b,\pm}\sin\left(\frac{\theta_{\vec{k}^{(n)}_{a,\pm}}+\theta_0}{2}\right) \\
&\times\sin\left((\overline{\vec{k}^{(n)}_{a,\pm}} - \vec{k}_b)\cdot\vec{r} + \theta_{\mathscr{R}^{(n)}_{a,\pm}} - \frac{\theta_0}{2}\right),
\end{aligned} \tag{C.6}$$

where $\Delta\theta_{\mathscr{R}^{(m,n)}_{a,b,\pm}} = \theta_{\mathscr{R}^{(m)}_{a,\pm}} - \theta_{\mathscr{R}^{(n)}_{b,\pm}}$.

Similarly, the components of $\vec{P}^{\pm}_{\mathscr{R},\vec{\sigma}}(\vec{r})$ are given by:

$$\begin{aligned}
P^{\pm}_{\mathscr{R},\hat{\sigma}_Z}(\vec{r}) &= -\sum_{a=1,2}\sum_{\substack{n,m\in\mathscr{N}_{a,\pm}\\ m<n}}\frac{k_a|\mathscr{R}^{(n)}_{a,\pm}\mathscr{R}^{(m)}_{a,\pm}|\,\sin(\phi^{(n,m)}_{a,a,\pm})}{\sqrt{k^{(n)}_{aX,\pm}k^{(m)}_{aX,\pm}}} \\
&\times\sin((\overline{\vec{k}^{(n)}_{a,\pm}} - \overline{\vec{k}^{(m)}_{a,\pm}})\cdot\vec{r} + \Delta\theta_{\mathscr{R}^{(n,m)}_{a,a,\pm}}) \\
&+ \sum_{n\in\mathscr{N}_{1,\pm}}\sum_{m\in\mathscr{N}_{2,\pm}}\frac{\sqrt{k_1k_2}\,|\mathscr{R}^{(n)}_{1,\pm}\mathscr{R}^{(m)}_{2,\pm}|\,\cos(\phi^{(n,m)}_{1,2,\pm})}{\sqrt{k^{(n)}_{1X,\pm}k^{(m)}_{2X,\pm}}} \\
&\times\cos((\overline{\vec{k}^{(n)}_{1,\pm}} - \overline{\vec{k}^{(m)}_{2,\pm}})\cdot\vec{r} + \Delta\theta_{\mathscr{R}^{(n,m)}_{1,2,\pm}}) \\
&- \sum_{(a,b)\in\{(1,-),(2,+)\}}\sum_{n\in\mathscr{N}_{a,\pm}}\sqrt{\frac{k_1k_2}{k^{(n)}_{aX,\pm}|\vec{k}_b\cdot\hat{x}|}}\,\delta_{b,\pm}\sin\left(\frac{\theta_{\vec{k}^{(n)}_{a,\pm}}+\theta_0}{2}\right) \\
&\times\sin\left((\overline{\vec{k}^{(n)}_{a,\pm}} - \vec{k}_b)\cdot\vec{r} + \theta_{\mathscr{R}^{(n)}_{a,\pm}} - \frac{\theta_0}{2}\right) \\
&+ \sum_{(a,b)\in\{(1,+),(2,-)\}}\sum_{n\in\mathscr{N}_{a,\pm}}\frac{k_a}{\sqrt{k^{(n)}_{aX,\pm}|\vec{k}_b\cdot\hat{x}|}}\,\delta_{b,\pm}\cos\left(\frac{\theta_{\vec{k}^{(n)}_{a,\pm}}+\theta_0}{2}\right) \\
&\times\cos\left((\overline{\vec{k}^{(n)}_{a,\pm}} - \vec{k}_b)\cdot\vec{r} + \theta_{\mathscr{R}^{(n)}_{a,\pm}} - \frac{\theta_0}{2}\right)
\end{aligned} \tag{C.7}$$

$$\begin{aligned}
P^{\pm}_{\mathscr{R},\hat{\sigma}_X}(\vec{r}) &= \pm\frac{\sin(\theta_0)k_{\pm}}{2|\vec{k}_{\pm}\cdot\hat{x}|} - \sum_{a=1,2}\sum_{n\in\mathscr{N}_{a,\pm}}(-1)^a\frac{k_a\,|\mathscr{R}^{(n)}_{a,\pm}|^2\sin(\theta_{\vec{k}^{(n)}_{a,\pm}})}{2k^{(n)}_{aX,\pm}} \\
&- \sum_{a=1,2}\sum_{\substack{n,m\in\mathscr{N}_{a,\pm}\\ m<n}}(-1)^a\frac{k_a|\mathscr{R}^{(n)}_{a,\pm}\mathscr{R}^{(m)}_{a,\pm}|\,\sin\left(\frac{\theta_{\vec{k}^{(n)}_{a,\pm}}+\theta_{\vec{k}^{(m)}_{a,\pm}}}{2}\right)}{\sqrt{k^{(n)}_{aX,\pm}k^{(m)}_{aX,\pm}}} \\
&\times\cos((\overline{\vec{k}^{(n)}_{a,\pm}} - \overline{\vec{k}^{(m)}_{a,\pm}})\cdot\vec{r} + \Delta\theta_{\mathscr{R}^{(n,m)}_{a,a,\pm}}) \\
&- \sum_{n\in\mathscr{N}_{1,\pm}}\sum_{m\in\mathscr{N}_{2,\pm}}\frac{\sqrt{k_1k_2}\,|\mathscr{R}^{(n)}_{1,\pm}\mathscr{R}^{(m)}_{2,\pm}|\,\cos\left(\frac{\theta_{\vec{k}^{(n)}_{1,\pm}}+\theta_{\vec{k}^{(m)}_{2,\pm}}}{2}\right)}{\sqrt{k^{(n)}_{1X,\pm}k^{(m)}_{2X,\pm}}} \\
&\times\sin((\overline{\vec{k}^{(n)}_{1,\pm}} - \overline{\vec{k}^{(m)}_{2,\pm}})\cdot\vec{r} + \Delta\theta_{\mathscr{R}^{(n,m)}_{1,2,\pm}}) \\
&- \sum_{(a,b)\in\{(1,-),(2,+)\}}\sum_{n\in\mathscr{N}_{a,\pm}}(-1)^a\sqrt{\frac{k_1k_2}{k^{(n)}_{aX,\pm}|\vec{k}_b\cdot\hat{x}|}}\,\delta_{b,\pm}\sin\left(\frac{\theta_{\vec{k}^{(n)}_{a,\pm}}+\theta_0}{2}\right) \\
&\times\cos\left((\overline{\vec{k}^{(n)}_{a,\pm}} - \vec{k}_b)\cdot\vec{r} + \theta_{\mathscr{R}^{(n)}_{a,\pm}} - \frac{\theta_0}{2}\right) \\
&+ \sum_{(a,b)\in\{(1,+),(2,-)\}}\sum_{n\in\mathscr{N}_{a,\pm}}(-1)^a\frac{k_a}{\sqrt{k^{(n)}_{aX,\pm}|\vec{k}_b\cdot\hat{x}|}}\,\delta_{b,\pm}\cos\left(\frac{\theta_{\vec{k}^{(n)}_{a,\pm}}+\theta_0}{2}\right) \\
&\times\sin\left((\overline{\vec{k}^{(n)}_{a,\pm}} - \vec{k}_b)\cdot\vec{r} + \theta_{\mathscr{R}^{(n)}_{a,\pm}} - \frac{\theta_0}{2}\right)
\end{aligned} \tag{C.8}$$

and

$$\begin{aligned}
P^{\pm}_{\mathscr{R},\hat{\sigma}_Y}(\vec{r}) &= \mp\frac{\cos(\theta_0)k_{\pm}}{2|\vec{k}_{\pm}\cdot\hat{x}|} + \sum_{a=1,2}\sum_{n\in\mathscr{N}_{a,\pm}}(-1)^a\frac{k_a\,|\mathscr{R}^{(n)}_{a,\pm}|^2\cos(\theta_{\vec{k}^{(n)}_{a,\pm}})}{2k^{(n)}_{aX,\pm}} \\
&- \sum_{a=1,2}\sum_{\substack{n,m\in\mathscr{N}_{a,\pm}\\ m<n}}(-1)^a\frac{k_a|\mathscr{R}^{(n)}_{a,\pm}\mathscr{R}^{(m)}_{a,\pm}|\,\cos\left(\frac{\theta_{\vec{k}^{(n)}_{a,\pm}}+\theta_{\vec{k}^{(m)}_{a,\pm}}}{2}\right)}{\sqrt{k^{(n)}_{aX,\pm}k^{(m)}_{aX,\pm}}} \\
&\times\cos((\overline{\vec{k}^{(n)}_{a,\pm}} - \overline{\vec{k}^{(m)}_{a,\pm}})\cdot\vec{r} + \Delta\theta_{\mathscr{R}^{(n,m)}_{a,a,\pm}}) \\
&+ \sum_{n\in\mathscr{N}_{1,\pm}}\sum_{m\in\mathscr{N}_{2,\pm}}\frac{\sqrt{k_1k_2}\,|\mathscr{R}^{(n)}_{1,\pm}\mathscr{R}^{(m)}_{2,\pm}|\,\sin\left(\frac{\theta_{\vec{k}^{(n)}_{1,\pm}}+\theta_{\vec{k}^{(m)}_{2,\pm}}}{2}\right)}{\sqrt{k^{(n)}_{1X,\pm}k^{(m)}_{2X,\pm}}} \\
&\times\sin((\overline{\vec{k}^{(n)}_{1,\pm}} - \overline{\vec{k}^{(m)}_{2,\pm}})\cdot\vec{r} + \Delta\theta_{\mathscr{R}^{(n,m)}_{1,2,\pm}}) \\
&- \sum_{(a,b)\in\{(1,-),(2,+)\}}\sum_{n\in\mathscr{N}_{a,\pm}}(-1)^a\sqrt{\frac{k_1k_2}{k^{(n)}_{aX,\pm}|\vec{k}_b\cdot\hat{x}|}}\,\delta_{b,\pm}\cos\left(\frac{\theta_{\vec{k}^{(n)}_{a,\pm}}+\theta_0}{2}\right) \\
&\times\cos\left((\overline{\vec{k}^{(n)}_{a,\pm}} - \vec{k}_b)\cdot\vec{r} + \theta_{\mathscr{R}^{(n)}_{a,\pm}} - \frac{\theta_0}{2}\right)
\end{aligned}$$

$$- \sum_{(a,b)\in\{(1,+),(2,-)\}} \sum_{n\in\mathcal{N}_{a,\pm}} (-1)^a \frac{k_a}{\sqrt{k^{(n)}_{aX,\pm}|\vec{k}_b\cdot\hat{x}|}} \delta_{b,\pm} \sin\left(\frac{\theta_{\vec{k}^{(n)}_{a,\pm}} + \theta_0}{2}\right) \times \sin\left((\vec{k}^{(n)}_{a,\pm} - \vec{k}_b)\cdot\vec{r} + \theta_{\mathscr{M}^{(n)}_{a,\pm}} - \frac{\theta_0}{2}\right). \tag{C.9}$$

ORCID iDs

Jamie D Walls https://orcid.org/0000-0003-4813-852X

References

[1] Beenakker C W J and van Houten H 1991 Quantum transport in semiconductor nanostructures *Solid State Phys.* **44** 1–228

[2] Crommie M F, Lutz C P and Eigler D M 1993 Confinement of electrons to quantum corrals on a metal-surface *Science* **262** 218–20

[3] Heller E J, Crommie M F, Lutz C P and Eigler D M 1994 Scattering and absorption of surface electron waves in quantum corrals *Nature* **369** 464–6

[4] Topinka M A, LeRoy B J, Shaw S E J, Heller E J, Westervelt R M, Maranowski K D and Gossard A C 2000 Imaging coherent electron flow from a quantum point contact *Science* **289** 2323–6

[5] Aidala K E, Parrott R E, Kramer T, Heller E J, Westervelt R M, Hanson M P and Gossard A C 2007 Imaging magnetic focusing of coherent electron waves *Nat. Phys.* **3** 464–8

[6] Talbot H F 1836 Facts relating to optical science *Phil. Mag.* **9** 401–7

[7] Rayleigh L 1881 On copying diffraction gratings and on some phenomenon connected therewith *Phil. Mag.* **11** 196–205

[8] Wen J, Zhang Y and Xiao M 2013 The Talbot effect: recent advances in classical optics, nonlinear optics, and quantum optics *Adv. Opt. Photonics* **5** 83–130

[9] Berry M, Marzoli I and Schleich W 2001 Quantum carpets, carpets of light *Phys. World* **14** 39–44

[10] Cronin A D and McMorran B 2006 Electron interferometry with nanogratings *Phys. Rev.* A **74** 061602(R)

[11] Chapman M S, Ekstrom C R, Hammond T D, Schmiedmayer J, Tannian B E, Wehinger S and Pritchard D E 1995 Near-field imaging of atom diffraction gratings: the atomic Talbot effect *Phys. Rev.* A **51** R14–7

[12] Hornberger K, Uttenthaler S, Brezger B, Hackermuller L, Arndt M and Zeilinger A 2003 Collisional decoherence observed in matter wave interferometry *Phys. Rev. Lett.* **90** 160401

[13] Dennis M R, Zheludev N L and Garcia de Abajo F J 2007 The plasmon Talbot effect *Opt. Express* **15** 9692–700

[14] Maradudin A A and Leskova T A 2009 The Talbot effect for a surface plasmon polariton *New J. Phys.* **11** 033004

[15] Tang W X, Paganin D M and Wan W 2012 Proposal for electron spin Talbot effect *Phys. Rev.* B **85** 064418

[16] Walls J D and Hadad D 2016 The Talbot effect for two-dimensional massless Dirac fermions *Sci. Rep.* **6** 26698

[17] Bychkov Y A and Rashba E I 1984 Oscillatory effects and the magnetic susceptibility of carriers in inversion layers *J. Phys. C: Solid State Phys.* **17** 6039–45

[18] Walls J D and Heller E J 2007 Spin-orbit induced interference effects in quantum corrals *Nano Lett.* **7** 3377–82

[19] Walls J D, Huang J, Westervelt R M and Heller E J 2006 Multiple-scattering theory for two-dimensional electron gases in the presence of spin–orbit coupling *Phys. Rev.* B **73** 035325

[20] Khomitsky D V 2007 Scattering on the lateral one-dimensional superlattice with spin–orbit coupling *Phys. Rev.* B **76** 033404

[21] Scheid M, Pfund A, Bercioux D and Richter K 2007 Coherent spin ratchets: a spin–orbit based quantum ratchet mechanism for spin-polarized currents in ballistic conductors *Phys. Rev.* B **76** 195303

[22] Smirnov S, Bercioux D and Grifoni M 2007 Bloch's theory in periodic structures with Rashba's spin–orbit interaction *EPL* **80** 27003

[23] Ang Y S, Ma Z and Zhang C 2015 Quantum ratchet in two-dimensional semiconductors with Rashba spin–orbit interaction *Sci. Rep.* **5** 7872

[24] Seibold G, Caprara S, Grilli M and Raimondi R 2015 Intrinsic spin Hall effect in systems with striped spin–orbit coupling *EPL* **112** 17004

[25] Henk J, Ernst A and Bruno P 2003 Spin polarization of the l-gap surface states on Au(111) *Phys. Rev.* B **68** 165416

[26] van Weperen I, Tarasinski B, Eeltink D, Pribiag V S, Plissard S R, Bakkers E P A M, Kouwenhoven L P and Wimmer M 2015 Spin–orbit interaction in InSb nanowires *Phys. Rev.* B **91** 201413(R)

[27] Kittel C 1987 *Quantum Theory of Solids* 2nd edn (New York: Wiley)

[28] Vaishnav J Y, Walls J D, Apratim M and Heller E J 2007 Matter-wave scattering and guiding by atomic arrays *Phys. Rev.* A **76** 013620

[29] Sanz A S and Miret-Artes S 2007 A causal look into the quantum Talbot effect *J. Chem. Phys.* **126** 234106

[30] Vaishnav J Y and Clark C W 2008 Observing zitterbewegung with ultracold atoms *Phys. Rev. Lett.* **100** 153002

[31] Plotnik Y, Bandres M A, Stutzer S, Lumer Y, Rechtsman M C, Szameit A and Segev M 2016 Analogue of Rashba pseudo-spin–orbit coupling in photonic lattices by gauge field engineering *Phys. Rev.* B **94** 020301(R)

[32] Dragoman D 2014 Optical analogues of nanostructures with Rashba–Dresselhaus interactions *J. Opt.* **16** 015710

[33] Nicorovici N A, McPhedran R C and Petit R 1994 Efficient calculation of the Green's function for electromagnetic scattering by gratings *Phys. Rev.* E **49** 4563–77

[34] Yasumoto K and Yoshitomi K 1999 Efficient calculation of lattice sums for free-space periodic Green's function *IEEE Trans. Antennas Propagat.* **47** 1050–5

[35] Walls J D and Hadad D 2015 Suppressing Klein tunneling in graphene using a one-dimensional array of localized scatterers *Sci. Rep.* **5** 8435

[36] MATLAB 2018 MATLAB 2018A release, The Mathworks Inc.

[37] Foldy L L 1945 The multiple scattering of waves *Phys. Rev.* **67** 107–19

[38] Lax M 1951 Multiple scattering of waves *Rev. Mod. Phys.* **23** 287–310